CVR-2025-0447: Cardiovascular risk and allostatic-interoception in dementia

Cardiovascular risk factors and the allostatic interoceptive network in dementia

Jessica L. Hazelton[1,2,3]*, Joaquín Migeot[1,4]*, Raul Gonzalez-Gomez[1], Florencia Altschuler[1,2], Claudia Duran-Aniotz[1], Olivia Wen[4], Dante Sebastián Galván Rial[1,5], Pablo Barttfeld[1,5], Vicente Medel[1], Cecilia González Campo[1,2], Ana María Castro-Laguardia[1], Hernán Hernández[1], Carolina Gonzalez-Silva[1], Olga Castaner[4,6], Kun Hu[7], Peng Li[7,8,9], María Isabel Behrens[10,11,12,13] #, Martin A. Bruno[14] #, Juan Felipe Cardona[15] #, Nilton Custodio[16] #, Hernando Santamaria-Garcia[17,18] #, Adolfo M. Garcia[2,4,19] #, Maria E. Godoy[1,2] #, José Alberto Avila-Funes[20] #, Marce Maito[1] #, Diana L. Matallana[21,22] #, Bruce Miller[23,24] #, Francisco Lopera[25] † #,Maira Okada de Oliveira[23,26] #, Stefanie D. Pina-Escudero[23,24] #, Katherine L. Possin[23,24] #, Elisa de Paula France Resende[23,27] #, Pablo Reyes[28] #, Andrea Slachevsky [29,30,31,32] #, Ana Luisa Sosa[33] # , Leonel T. Takada[25] #, Jennifer S. Yokoyama[23,24,34] #, Agustín Ibanez[1,2,4]

*These authors contributed equally to this work.

† Professor Francisco Lopera passed away on the 10th of September 2024

Alphabetical order

Affiliations:

1. Latin American Brain Health Institute (BrainLat), Universidad Adolfo Ibáñez, Santiago, Chile.
2. Cognitive Neuroscience Center (CNC), Universidad de San Andrés, Buenos Aires, Argentina.
3. The University of Sydney, Brain and Mind Centre, School of Psychology, Sydney, Australia.
4. Global Brain Health Institute (GBHI), University of California San Francisco (UCSF), California, US; & Trinity College Dublin, Dublin, Ireland.
5. Cognitive Science Group. Instituto de Investigaciones Psicológicas (IIPsi, CONICET-UNC), Facultad de Psicología, Universidad Nacional de Córdoba, Córdoba, Argentina.
6. Cardiovascular risk and Nutrition Research Group. Hospital del Mar Research Institute, Spain; CIBER Epidemiology and Public Health (CIBERESP), ISCIII, Spain.
7. Department of Anesthesia, Critical Care and Pain Medicine, Massachusetts General Hospital, Harvard Medical School, Boston, Massachusetts, USA.
8. Division of Sleep Medicine, Harvard Medical School, Boston, MA, USA.
9. Division of Sleep and Circadian Disorders, Brigham and Women's Hospital, Harvard Medical School, Boston, MA, USA.
10. Departamento de Neurociencia, Facultad de Medicina, Universidad de Chile, Santiago, Chile.
11. Departamento de Neurología y Neurocirugía, Hospital Clínico Universidad de Chile.
12. Centro de Investigación Clínica Avanzada (CICA), Universidad de Chile, Santiago, Chile.
13. Servicio de Neurología, Departamento de Medicina, Clínica Alemana-Universidad del Desarrollo, Santiago de Chile, Chile.
14. Instituto de Ciencias Biomédicas, Universidad Católica de Cuyo, San Juan, Argentina.
15. Facultad de Psicología, Universidad del Valle, Cali, Colombia.

16. Unit Cognitive Impairment and Dementia Prevention, Peruvian Institute of Neurosciences, Lima, Peru.
17. Pontificia Universidad Javeriana, PhD program of Neuroscience, Bogotá, Colombia.
18. Hospital Universitario San Ignacio, Centro de Memoria y Cognición Intellectus, Bogotá, Colombia.
19. Departamento de Lingüística y Literatura, Universidad de Santiago de Chile, Santiago, Chile.
20. Dirección de Enseñanza, Instituto Nacional de Ciencias Médicas y Nutrición Salvador Zubirán, Mexico City, Mexico.
21. Instituto de Envejecimiento, Facultad de Medicina, Pontificia Universidad Javeriana, Bogotá D.C., Colombia.
22. Center for Memory and Cognition, Hospital Universitario San Ignacio Bogotá, San Ignacio, Bogotá D.C., Colombia.
23. Global Brain Health Institute, University of California, San Francisco, California, USA
24. Memory and Aging Center, Department of Neurology, University of California, San Francisco, California, USA.
25. Grupo de Neurociencias de Antioquia, University of Antioquia, Medellín, Colombia
26. Cognitive Neurology and Behavioral Unit (GNCC), University of São Paulo, São Paulo, Brazil.
27. Universidade Federal de Minas Gerais, Belo Horizonte, Minas Gerais, Brazil
28. Instituto de Envejecimiento, Facultad de Medicina, Pontificia Universidad Javeriana, Bogotá D.C., Colombia
29. Faculty of Medicine, University of Chile, Santiago, Chile
30. Geroscience Center for Brain Health and Metabolism (GERO), Santiago de Chile, Chile
31. Memory and Neuropsychiatric Center (CMYN), Neurology Department, Hospital del Salvador
32. Servicio de Neurología, Departamento de Medicina, Clínica Alemana-Universidad del Desarrollo, Santiago de Chile, Chile
33. Laboratorio de Demencias del Instituto Nacional de Neurología y Neurocirugía Manuel Velasco Suárez, Mexico City, CDMX, México
34. Department of Radiology and Biomedical Imaging, University of California, San Francisco, San Francisco, CA 94158, USA.

Correspondence: Professor Agustin Ibáñez
Email: agustin.ibanez@gbhi.org
Latin American Brain Health Institute (BrainLat), Universidad Adolfo Ibanez, Chile

Abstract

Aims

Cardiovascular risk factors, such diabetes, hypertension, blood pressure, obesity, and smoking, are linked with allostatic-interoception – the continuous monitoring of internal bodily states in anticipation of environmental demands. These risk factors are associated with dementia risk. How these factors affect brain networks vulnerable to neurodegeneration and involved in allostatic-interoception, such as the Allostatic-Interoceptive Network (AIN), is unknown. We investigated the relationship between cardiovascular risk and AIN structure and function in frontotemporal lobar degeneration (FTLD) and Alzheimer's disease (AD).

Methods

We recruited 1501 participants (304 with FTLD, 512 with AD, and 685 healthy controls) from the Multi-Partner Consortium to Expand Dementia Research in Latin America (ReDLat). A cardiovascular risk score was calculated based on: age, sex, diabetes, hypertension, systolic blood pressure, body mass index, and smoking status. Cardiovascular risk was associated with gray matter integrity and functional connectivity in age- and sex-matched patient-control groups focusing on predefined regions of interest within the AIN.

Results

Higher cardiovascular risk was associated with reduced structural integrity and functional connectivity within the AIN in both FTLD and AD. FTLD patients showed more extensive structural and functional connectivity disruptions throughout the AIN. In AD patients, structural reductions in the AIN were prominent, with functional connectivity restricted to the hippocampus, parahippocampal gyrus, and orbitofrontal regions

Conclusions

Cardiovascular risk factors appear to adversely impact the AIN structure and function, with disease-specific patterns of vulnerability. Results underscore the importance of integrating

cardiovascular health into models of neurodegenerative disease and managing cardiovascular health to support brain integrity in dementia.

1 Introduction

Cardiovascular risk factors, including diabetes, hypertension, blood pressure, obesity, and smoking, are strongly associated with an increased risk of developing dementia (1) contributing to neurodegeneration through heightened vascular burden (2). Emerging synergistic approaches to brain health and disease call for the integration of comorbidities such as cardiovascular risk factors in understanding dementia (3, 4). Indeed, population-based studies indicate that individuals with cardiovascular comorbidities are five times more likely to develop all-cause dementia, with this risk being independent of Alzheimer's disease (AD)-related genetic predispositions (5). However, the specific impact of cardiovascular risk factors on brain networks vulnerable to dementia remains poorly understood.

The predictive coding theory of allostatic interoception (6, 7) states that the brain anticipates and processes internal bodily signals to adapt to environmental demands (6-13). Allostatic overload arises when the body's adaptive capacity is depleted over time due to chronic stress or environmental pressures (6, 7, 11). Cardiovascular function and allostatic-interoception are deeply interdependent (14-16). Higher allostatic load as measured by a composite score of cardiometabolic factors – such as blood pressure, body composition, cholesterol levels, and cortisol – has been linked to adverse aging outcomes (17). Despite the connection between cardiovascular risk and allostatic-interoception, no study has examined how cardiovascular risk factors influence brain networks particularly vulnerable to dementia.

Emerging evidence has shown that dysfunction in allostatic-interoception, encompassing behavioral, peripheral, and neural measures, are observed in frontotemporal lobar degeneration (FTLD) syndromes (13, 18-27), particularly in behavioral variant frontotemporal dementia (bvFTD). While evidence for interoceptive impairment in AD is mixed (18, 19, but see 22), altered allostatic markers have been consistently reported (26, 28-31). Allostatic-interoception is supported by the allostatic-interoceptive network (AIN), a

large-scale brain network that includes cortical and subcortical structures (e.g., insula, anterior cingulate cortex, orbitofrontal cortex, amygdala, hippocampus, parahippocampus, and thalamus)(6, 7, 18). Disruptions in the structural and functional integrity of the AIN have been documented in both FTLD and AD (18). However, the relationship between cardiovascular risk factors and changes in the AIN in dementia remains largely unexplored.

Taken together, this evidence suggests a hypothesis: cardiovascular risk factors may influence the AIN in dementia (6-8, 32, 33). Majority of studies to date, however, have predominantly focused on total gray matter volume (32-34), which does not provide a measure of specific brain structures associated with cardiovascular risk. Whilst some studies have focused on a limited subset of brain regions (e.g., hippocampus), these have been conducted in healthy adults or aging populations (32, 33, 35, 36) limiting their application to dementia populations. Critically, no study has investigated how cardiovascular risk factors may influence both structural and functional changes in the brain within AIN, a key network that we propose is related to cardiovascular risk. Further, no study has examined how cardiovascular risk factors contribute to neurodegeneration in dementia syndromes such as FTLD and AD, where allostatic-interoception dysfunction has been reported (18-22, 27). Further, to our knowledge, this association has not been investigated in Latin America, where cardiovascular risk factors are increased in the general population (37-39). Understanding how cardiovascular risk factors may relate to underlying neural mechanisms in dementia syndromes will further refine our understanding of these diseases and may bolster future precision medicine approaches by reducing comorbid risk factors.

In the current study, we recruited a Latin American and US cohort (N = 1501) from the Multi-Partner Consortium to Expand Dementia Research in Latin America (ReDLat)(31, 32). We investigated cardiovascular risk factors (e.g., diabetes, hypertension, systolic blood pressure, body mass index, and current smoking status) using the non-laboratory-based

Framingham's Risk Score (FRS)(40). We investigated the FRS alongside both structural and functional brain connectivity measures. Despite differences in allostatic-interoception and cardiovascular risk profiles in each dementia syndrome, we hypothesized that reduced structural and functional connectivity within the AIN would be associated with greater cardiovascular risk factors in both dementia syndromes, as evidence of an underlying neurobiological mechanism contributing to both processes.

2 Methods

2.1 Participants

The experimental workflow is shown in Figure 1. We recruited 1501 participants, including 304 FTLD patients, 512 AD patients, and 685 healthy controls (CN) from both Latin America and the United States (Supplementary Table 1-2 for subtype-specific information). All participants were recruited through ReDLat's ongoing multicenter protocols (41, 42) involving clinical examination, neuropsychological testing, and magnetic resonance imaging (MRI). Patients were diagnosed with FTLD syndromes based on the current sets of diagnostic criteria, including prominent changes to behavior, personality and/or language (43, 44), and motor features (45-47). AD syndrome was diagnosed based on current sets of diagnostic criteria, including typical AD with an amnestic profile (48) and atypical variants based on language features (43), visual features (49), and behavior (50). All CNs scored >24 on the Mini Mental State Examination (MMSE)(51, 52). Exclusion criteria included presence of major primary cardiovascular compromise (i.e., cardiovascular disease), history of other neurological disorders, psychiatric conditions, or substance abuse. CNs were demographically matched (i.e., age and sex matched) to each patient group (FTLD or AD) using R MatchIt to create disease-control groups for comparison (53), due to demographic differences between patient groups and controls in the full dataset. Approximately 10% of AD cases were also removed during the matching process due to older age (> 85 years of

age). All participants or their caregivers provided informed consent in line with the Declaration of Helsinki. The study was approved by the Ethics Committees of the involved institutions.

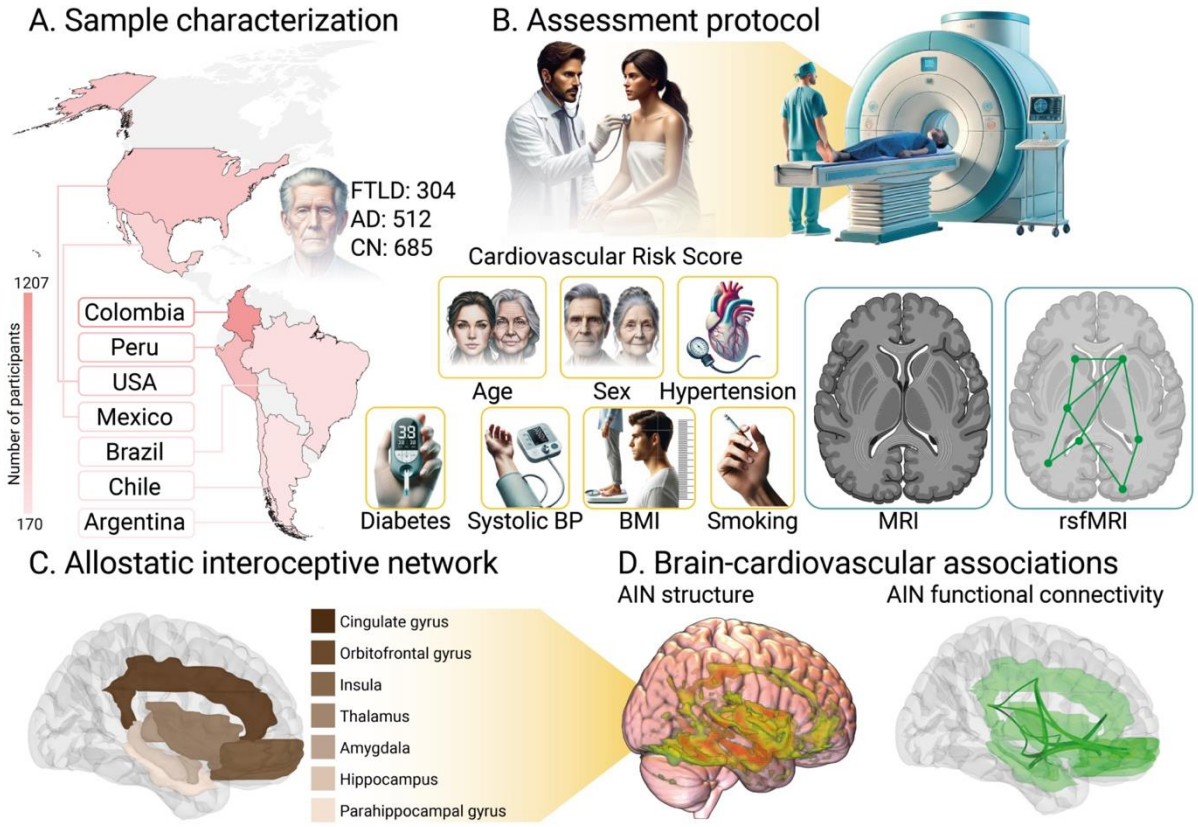

Figure 1. Experimental workflow. A) Sample characterization per country. Color bars indicate the number of participants. Circle plots represent the proportion of participants in each group. B) Assessment protocol. All participants underwent a clinical examination and had an MRI scan. The Framingham Risk Score (FRS) was calculated based on established non-laboratory measures, considering Age, Sex, Presence of Diabetes, Presence of Hypertension, Systolic blood pressure, Body mass index (BMI), and current smoking status. MRI measures included structural T1 MRI and resting state functional MRI (rsFMRI). C). Allostatic interoceptive network (AIN) regions investigated in the neuroimaging analyses. D) Brain-cardiovascular associations using the FRS were investigated in the AIN using structural voxel-based morphometry and functional connectivity analyses.

2.2 Measures

2.2.1 Cognition

The Mini Mental State Examination (MMSE) was used to measure cognitive performance based on measures of attention, memory, language, and visuospatial abilities (52). Total MMSE scores are out of 30, with higher scores representing better performance.

2.2.2 Disease severity

Two measures of disease severity were calculated: 1) The Clinical Dementia Rating (CDR) in AD, and 2) the Clinical Dementia Rating scale – FTLD (CDR-FTLD) in FTLD. In brief, both measures assess functionality using a semi-structured interview with patients and their informants and cover six domains including memory, orientation, problem solving/judgment, community affairs, home and hobbies, and personal care (54). In addition, the CDR-FTLD includes measures of behavior relevant for FTLD patients (55). The CDR-SOB (Sum of Boxes) is calculated by summing each of the domain scores. Higher CDR-SOB scores represent greater functional impairment.

2.2.3 Cardiovascular risk

The Framingham's Risk Score (FRS) was calculated based on non-laboratory to measure cardiovascular risk (40). This score is previously validated (40), and measures cardiovascular risk based on age, biological sex (assigned male or female at birth), body mass index (BMI), systolic blood pressure, hypertension status (anti-hypertensive medication use and/or clinical report), diabetes status (diabetic medication and/or clinical report), and current smoking status (40)(Supplementary Table 3). High agreement between the non-laboratory-based and laboratory-based versions of the FRS has been reported (56-59). In brief, each measure is scored following previously validated guidelines, taking into account biological sex differences in cardiovascular risk (40). Higher FRS scores represent greater cardiovascular risk. Missing data were present in less than 10% of each variable necessary to calculate the

FRS and were evenly distributed across groups. To handle missing data, we employed multiple imputation using the MICE (Multivariate Imputation by Chained Equations) package in R (60).

2.3 Neuroimaging acquisition

Whole-brain structural MRI and resting-state functional MRI data were obtained, and standard pre-processing steps were followed as recommended by the Organization for Human Mapping (61, 62). Each center followed standard protocols (Supplementary Tables 4-5 scanner details and acquisitions).

2.4 Statistical analyses

2.4.1 Demographics

Demographic, neuropsychological, and cardiovascular risk variables were compared via t-tests (i.e., age, education, cognition, cardiovascular risk), or chi-square tests (i.e., biological sex). All behavioral analyses were conducted using Python (v.3.10.12) with Pandas package (v.2.0.3)(63) and Statsmodel package (v.0.14.2)(64).

2.4.2 Voxel-based morphometry

Voxel-based morphometry (VBM) was performed using the Computational Anatomy Toolbox (CAT12, https://neuro-jena.github.io/cat/) in MATLAB R2022a. Standard pre-processing steps were followed, including bias-field correction, noise reduction, skull stripping, segmentation, and normalization to the Montreal Neurological Institute (MNI) space with a resolution of 1.5 isotropic, using default parameters. Sample homogeneity and orthogonality checks were performed. Regions of interest (ROI) masks were created using the MarsBar toolbox (65) for the AIN (insula, anterior cingulate cortex, mid cingulate cortex, orbitofrontal cortex, amygdala, hippocampus, parahippocampus, and thalamus)(7, 8, 18) using the Automated Anatomical Labeling (AAL-2) atlas (66). Pearson correlations were conducted between TIV-corrected GM volume and cardiovascular risk. Within the AIN,

regression analyses were conducted with the FRS score, controlling for group (FTLD vs CN; AD vs CN), scanner, and total intracranial volume. To directly compare our AD and FTLD groups, we transformed our pre-processed data by transforming the normalized and smoothed outputs to w-scored images (67-70). Here, w-scores (Mean = 0, Standard deviation = 1) show how different the observed GM volume in each voxel is (e.g., positive or negative w-score) than expected, based on an individual's global composite score adjusted for specific covariates (e.g., age, sex, diagnosis, total intracranial volume, and scanner type). This approach has been previously used in neurodegenerative studies to account for demographic differences and scanner effects without losing information regarding diagnostic effects (67-70). The resulting w-score maps of each individual were used for the direct comparison between AD and FTLD. Here, regression analyses were conducted with the FRS score and the interaction between FRS score and diagnosis (AD vs FTLD) was entered into the model. All clusters are reported using threshold-free cluster enhancement, at FDR-corrected, $p<.05$ with a contiguous threshold of 50 voxels.

2.4.3 Resting-state functional connectivity

All data were pre-processed following a standard pipeline in CONN (22.a) (60, 61) using SPM (v.12)(71)(Supplementary methods). In brief, preprocessing steps involved spatial convolution smoothing with a Gaussian kernel of 6 mm full width half maximum (FWHM). Next, functional data were denoised using a standardized denoising pipeline in CONN (72). We focused our analyses on ROI-to-ROI functional connectivity between regions within the AIN (7, 8, 18), mirroring the masks outlined in our structural analyses for comparison (Supplementary materials for further details). Group-level analyses were performed using a General Linear Model (GLM)(72). For each individual connection a separate GLM was estimated, with first-level connectivity measures at this connection as dependent variables, and FRS as independent variable, with scanner and group as a covariate. Connection-level

hypotheses were evaluated using multivariate parametric statistics with random-effects across subjects and sample covariance estimation across multiple measurements. Inferences were performed at the level of individual clusters (groups of similar connections). Cluster-level inferences were based on parametric statistics within- and between- each pair of networks (Functional Network Connectivity)(73), with networks identified using a complete-linkage hierarchical clustering procedure based on ROI-to-ROI anatomical proximity and functional similarity metrics (72). Results were reported using familywise corrected *p*-FDR < 0.05 connection- and cluster-level threshold (74). To directly compare the effects of the association between the FRS and functional connectivity between AD and FTLD, we applied a subsampling framework (75, 76) to the subset of connections that were statistically significant in either AD or FTLD models (n = 15). We conducted 1000 iterations of stratified random subsampling for each connection without replacement. In each iteration, we fitted an ordinary least squares (OLS) regression model predicting functioning connectivity from FRS scores, while adjusting for age, sex, and scanner type. The t-value associated with the RS coefficient was extracted from each model and stored, yielding empirical distributions of t-values for AD and FTLD, representing the variability of the FRS-functional connectivity associations across groups. Next, we performed independent sample t-tests to compare the distribution of t-values, allowing us to test the differential impact of FRS on functional connectivity between AD and FTLD.

2.5 Data availability statement

Anonymized data that support the study findings are drawn from the BrainLat project (41), a large open access multimodal neuroimaging database that can be found here: https://www.synapse.org/Synapse:syn51549340/wiki/624187 (77).

3 Results

3.1 Demographics, cognitive performance and cardiovascular risk

No significant differences were observed between age and sex between FTLD and CN or AD and CN following matching (Table 1, Supplementary Tables 1-2 for subtype analyses). In both tandems (FTLD-CN, and AD-CN), patients had worse cognitive scores than the controls (both *p*'s <.001). FTLD and AD were in mild-to-moderate disease stages, on average. Cardiovascular risk scores did not differ between patients with dementia syndromes and CN tandems (both *p*'s > 05).

Table 1. Demographic and neuropsychological assessment between patients and control tandems.

	CN (n = 304)	FTLD (n = 304)	Statistic	*p*
Age	64.77 ± 8.60	65.44 ± 7.86	-0.99	0.320
Sex (M:F)	166:138	166:138	0.00	1.000
Education	14.56 ± 5.46	14.21 ± 4.15	0.85	0.395
MMSE	28.14 ± 3.00	21.52 ± 6.47	15.97	<.001
CDR-FTLD SoB	-	8.64 ± 3.97	-	-
FRS	13.67 ± 3.99	13.80 ± 3.84	-0.40	0.687
	CN (n = 432)	AD (n = 429)	Statistic	*p*
Age	67.68 ± 7.25	68.33 ± 7.54	1.29	0.195
Sex (M:F)	145:287	151:278	0.19	0.665
Education	13.27 ± 5.92	12.92 ± 4.92	-0.96	0.335
MMSE	27.50 ± 3.36	19.92 ± 4.92	-23.40	<.001
CDR SoB	-	5.82 ± 2.98	-	-
FRS	14.54 ± 3.90	15.01 ± 4.14	1.70	0.090

Note. Abbreviations: AD = Alzheimer's disease; CDR-SoB = Clinical Dementia Rating Sum of Boxes; CN = controls; FRS = Framingham's Risk Score; FTLD = frontotemporal lobar degeneration; MMSE = Mini Mental State Examination

3.2 Increased cardiovascular risk is associated with reduced structural integrity of the AIN in dementia

Expected patterns of atrophy were observed in each clinical syndrome compared to CNs (Supplementary Figures 1-2; Supplementary Tables 6-16).

In FTLD, higher cardiovascular risk was associated with reduced structural integrity of the bilateral insula, thalamus, anterior cingulate cortex, and paracingulate cortex, and right amygdala, hippocampus, parahippocampus, temporal pole, and superior temporal gyrus. (Figure 2A, Supplementary Table 16). Similar results were observed when controlling for FTD subtype (Supplementary Table 17).

In AD, higher cardiovascular risk scores were associated with reduced structural integrity of the bilateral amygdala, hippocampus, parahippocampal gyrus, superior temporal gyrus, temporal pole, insula, thalamus, anterior cingulate cortex, and paracingulate cortex (Figure 2B, Supplementary Table 18). Similar results were observed when controlling for AD subtype (Supplementary Table 19).

Direct comparisons between AD and FTLD after accounting for age and sex revealed that increased cardiovascular risk was associated with reduced grey matter integrity in key AIN regions (e.g., bilateral ACC, right insula) in FTLD compared to AD (Figure 3A, Supplementary Table 20). No clusters were observed where increased cardiovascular risk was associated with reduced grey matter integrity in AD compared to FTLD (Figure 3B).

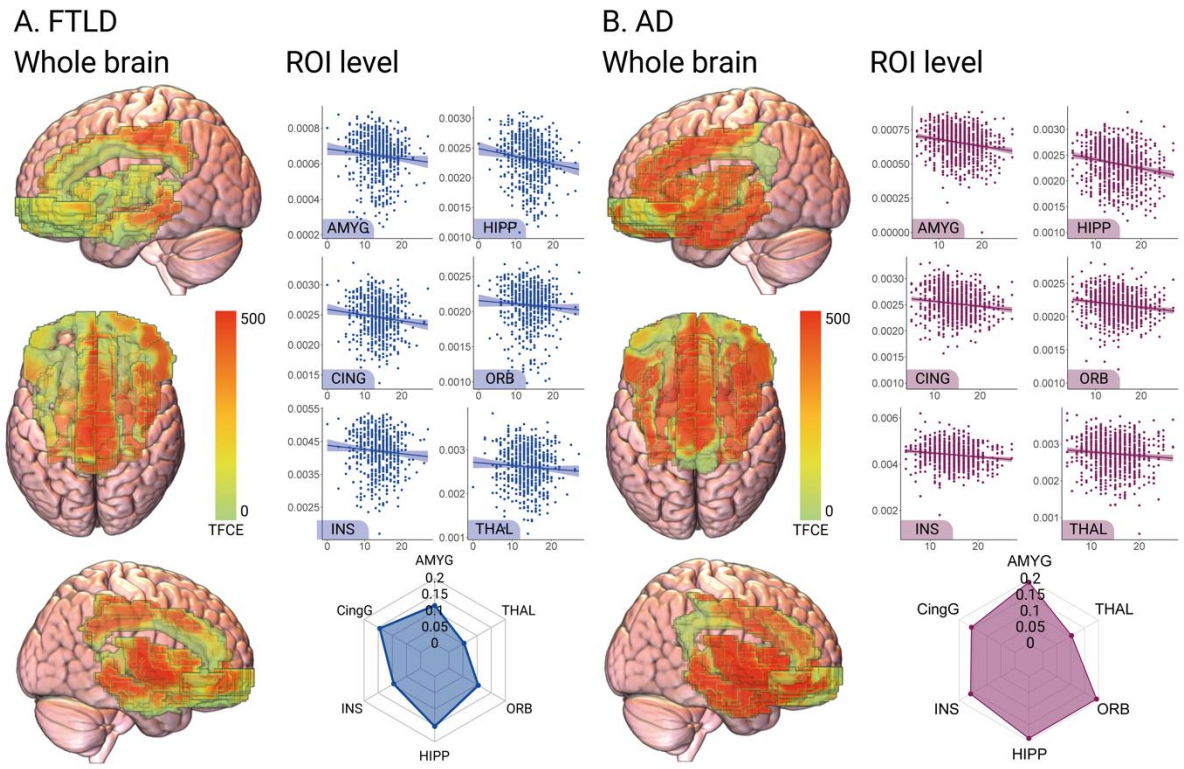

Figure 2. Brain volume of the allostatic interoceptive network and cardiovascular risk in dementia. Reduced structural integrity associated with increased cardiovascular risk in A) FTLD syndromes and B) in AD syndromes. Whole brain plots display VBM results with TFCE values shown within predefined regions, with FDR $p<.05$. Scatterplots show GM volumes within predefined regions associated with cardiovascular risk scores. Spider plots display Pearson *r*-values for correlations between each ROI and FRS score. Abbreviations: AMYG: Amygdala; CING: Cingulate; HIPP: Hippocampus; INS: Insula; ORB: Orbitofrontal cortex; THAL: Thalamus; FTLD: Frontotemporal Lobar Degeneration; AD: Alzheimer's disease.

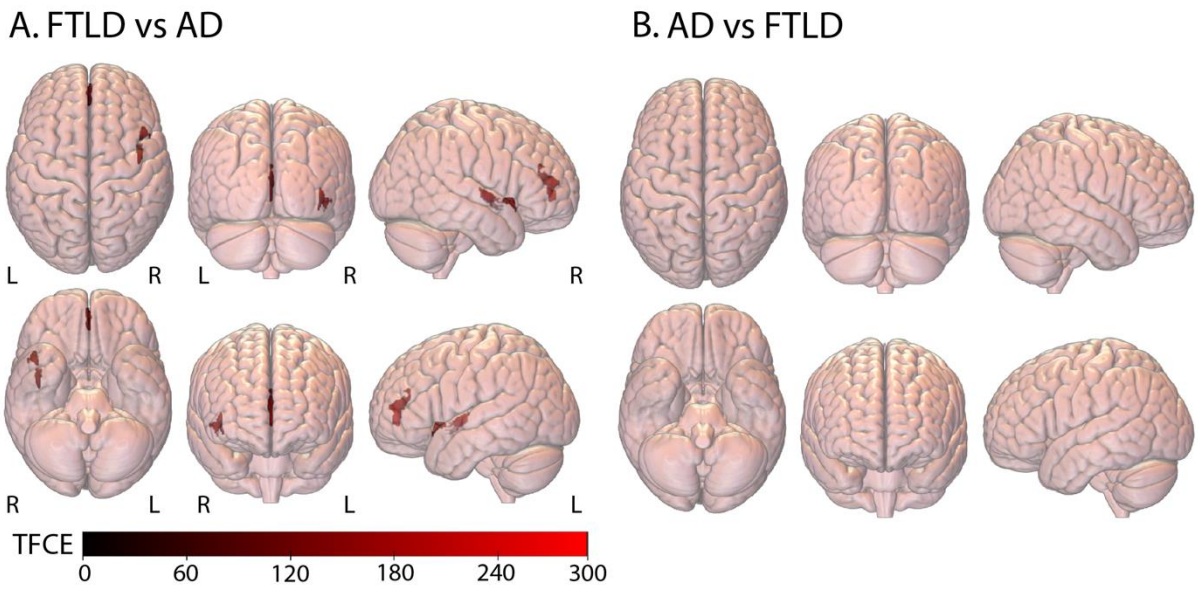

Figure 3. Reduced grey matter integrity associated with increased cardiovascular risk in A) FTLD vs AD, and B) AD vs FTLD. Whole brain plots display VBM results with TFCE values shown in predefined regions, with FDR $p<.05$ using a 50 contiguous voxel threshold.

3.3 Increased cardiovascular risk is associated with reduced AIN connectivity in dementia

In FTLD, higher cardiovascular risk was associated with reduced resting-state functional connectivity in six clusters in FTLD (Figure 4A, Supplementary Table 20), including the bilateral insula (cluster 1), bilateral thalamus (cluster 2), bilateral parahippocampal gyrus, orbitofrontal cortex (medial part), and bilateral hippocampus (cluster 3), bilateral parahippocampal gyrus and orbitofrontal cortex (inferior, superior, and middle parts)(cluster 4), bilateral middle cingulate cortex and bilateral posterior cingulate cortex (cluster 5) and bilateral orbitofrontal cortex (medial part)(cluster 6).

In AD, higher cardiovascular risk was associated with reduced resting-state functional connectivity in two clusters, involving bilateral parahippocampal gyrus, orbitofrontal cortex (medial part) and hippocampus (cluster 1), and the bilateral parahippocampal gyrus and orbitofrontal cortex (middle and superior)(cluster 2)(Figure 4B, Supplementary Table 21).

Finally, we compared functional connectivity in FTLD and AD directly, based on the significant connections observed in each group separate (n = 15 connections). Here, a stronger effect was observed for higher cardiovascular risk in FTLD than in AD for 14/15 of the connections (Table 2), including reduced connectivity between the bilateral orbitofrontal cortex, hippocampus, parahippocampus, insula, and the left middle and posterior cingulate cortex. The reverse pattern was observed for one connection, where a stronger effect for higher cardiovascular risk was observed in AD than in FTLD in the right orbitofrontal cortex and left parahippocampal gyrus. These results largely mirror the pattern of results observed in the groups separately.

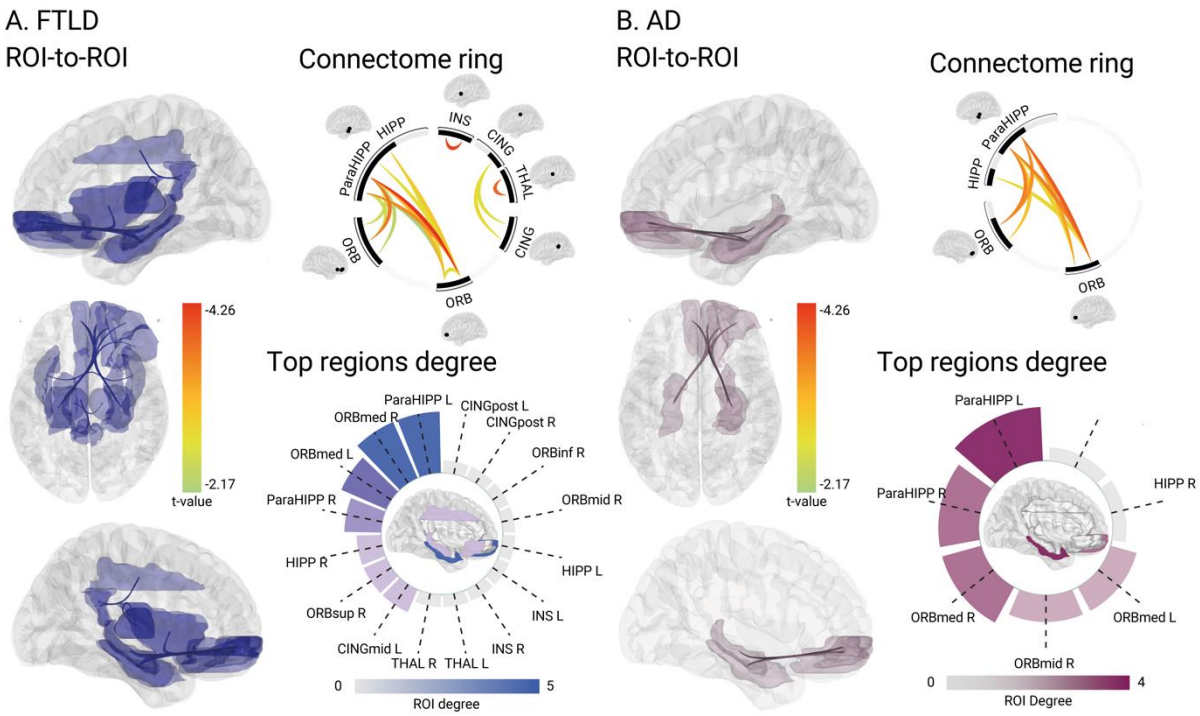

Figure 4. Allostatic interoceptive network functionality and cardiovascular risk in dementia. Reduced functional connectivity associated with increased cardiovascular risk in A) FTLD syndromes; and B) AD syndromes. In each panel, ROI-to-ROI connectivity maps are shown. Connectome rings show the strength of connectivity between each ROI, with color bars representing the connectivity strength using t-values. Radial plots show the number of connections of each ROI to different regions, with color bars representing the maximum number of ROI connections. Abbreviations: CINGmid: Middle cingulate cortex; CINGpost: Posterior cingulate cortex; HIPP: Hippocampus; INS: Insula; ORBinf: Orbitofrontal cortex (inferior); ORBmed: Orbitofrontal cortex (medial); ORBmid: Orbitofrontal cortex (middle); ORBsup: Orbitofrontal cortex (superior); ParaHIPP: Parahippocampal gyrus; THAL: Thalamus.

Table 2. Functional connectivity comparisons between FTLD and AD using 1000 subsampling models per group.

Connection	FTLD M ± SD	AD M ± SD	*t*	*P*
Frontal Med Orb R & Hippocampus L	-1.64 ± 0.80	-0.18 ± 0.82	-40.48	<.0.000001
Frontal Med Orb L & Hippocampus L	-1.34 ± 0.80	0.08 ± 0.81	-39.35	<.0.000001
Cingulum Mid L & Cingulum Post L	-2.09 ± 0.76	-0.64 ± 0.89	-39.09	<.0.000001
Thalamus L & Thalamus R	-1.48 ± 0.79	-0.41 ± 0.89	-28.29	<.0.000001
Frontal Med Orb R & Parahippocampal L	-1.99 ± 0.75	-1.01 ± 0.85	-27.15	<.0.000001
Frontal Sup Orb R & Parahippocampal L	-1.42 ± 0.69	-0.68 ± 0.79	-22.51	<.0.000001
Cingulum Mid L & Cingulum Post R	-1.50 ± 0.77	-0.69 ± 0.84	-22.46	<.0.000001
Frontal Med Orb L & Parahippocampal L	-1.67 ± 0.84	-0.95 ± 0.84	-19.16	<.0.000001
Insula L & Insula R	-1.34 ± 0.75	-0.64 ± 0.98	-17.95	<.0.000001
Frontal Med Orb L & Hippocampus R	-1.12 ± 0.77	-0.50 ± 0.85	-17.18	<.0.000001
Frontal Med Orb R & Parahippocampal R	-1.56 ± 0.75	-0.93 ± 0.91	-16.99	<.0.000001
Frontal Sup Orb R & Parahippocampal R	-0.64 ± 0.70	-0.11 ± 0.73	-16.57	<.0.000001
Frontal Inf Orb R & Parahippocampal L	-0.87 ± 0.80	-0.41 ± 0.85	-12.38	<.0.000001
Frontal Med Orb R & Hippocampus R	-1.00 ± 0.76	-0.83 ± 0.82	-4.77	0.000002
Frontal Mid Orb R & Parahippocampal L	-0.72 ± 0.71	-1.00 ± 0.80	8.12	<.0.000001

Note. Subsampling for each group N = 1000, degrees of freedom (df) for each comparison = 1000. Abbreviations: AD, Alzheimer's Disease, FTLD, Frontotemporal Dementia, M, Mean, SD, Standard deviation.

4 Discussion

Our study provides the first evidence that cardiovascular risk factors are associated with substantial structural and functional features within the AIN in both FTLD and AD. While higher cardiovascular risk correlated with reduced structural integrity in similar brain regions of the AIN in both FTLD and AD, differences were observed in functional connectivity metrics, highlighting disease-specific network vulnerabilities. In FTLD, widespread reduced functional connectivity associated with greater cardiovascular risk was observed in the bilateral insula, cingulate cortex, orbitofrontal cortex, thalamus, and hippocampus, mirroring structural correlates. In AD, reduced connectivity was circumscribed within the hippocampus, parahippocampus, and orbitofrontal cortices. Further, direct comparisons between disease phenotypes revealed a stronger effect associated with cardiovascular risk in FTLD than in AD in both structural and functional analyses, when accounting for demographic differences. Our findings highlight similar structural burdens associated with cardiovascular risk, but the observed disease-specific functional alterations suggest that distinct pathways and network vulnerabilities are involved in cardiovascular risk in FTLD and AD. In the following paragraphs, we will consider the theoretical and clinical implications of this work, as well as the relevance for public policy and health initiatives to promote dementia prevention and improve dementia care.

Both structural and functional alterations within the AIN were associated with cardiovascular risk factors in FTLD and AD, which remained significant when considering disease subtypes within each syndrome. In FTLD, widespread structural and functional connectivity alterations were associated with cardiovascular risk in the AIN. This finding fits with emerging evidence of multimodal allostatic-interoceptive disruptions spanning behavioral, peripheral, and neural measures occurring within this syndrome, particularly within bvFTD (13, 18-25, 27). Taken together, this evidence suggests that allostatic overload likely influences and

exacerbates disease mechanisms in FTLD syndromes, based on observed damage within the AIN (6, 7, 18). Somewhat surprisingly, in AD increased cardiovascular risk was also associated with widespread structural volume reductions in the AIN, whereas functional neuroimaging analyses in AD revealed a more targeted pattern of connectivity disruptions in select AIN regions, such as the hippocampus, parahippocampus, and orbitofrontal cortex. Prior studies have reported altered allostatic markers in AD (26, 28-31), noting that cardiometabolic burden may have a more substantial impact on AD risk than genetic factors (5). Therefore, a plausible mechanism underlying this disruption in AD is impaired insulin signaling in the brain (29). Impaired insulin signaling has a bidirectional relationship with allostatic load and has been proposed to exacerbate AD pathophysiology (29), particularly within the hippocampus (78) and in more vulnerable populations (29) similar to our patient cohort. In sum, our findings support the predictive coding theory of allostatic interoception (6-11), by showing that cardiovascular stress potentially disrupts the brain's adaptive mechanisms likely via prolonged allostatic overload in both FTLD and AD. Further, reduced AIN connectivity and structural atrophy in FTLD and AD suggest that cardiovascular risks may hasten neurodegeneration by impairing interoceptive and emotional processing pathways (6, 7, 13, 18)

The current work has several strengths. First, cardiovascular health was associated with brain structure and function in two distinct dementia syndromes within the AIN, even in the absence of major cardiovascular compromise (i.e., no differences were observed in cardiovascular risk between controls and patients). This study extends on previous literature focusing on cardiovascular risk and hippocampal volume in healthy aging (32, 33) and highlights how cardiovascular burden manifests in disruptions in AIN structure and function in dementia. Further, our results support synergistic embodied health approaches that consider whole-body

health in brain health (3, 4). Routine cardiovascular assessments in clinical settings could be a valuable and actionable addition to dementia care and prognosis (79). Indeed, mid-life cardiovascular risk factors are among the strongest predictors of later life dementia (1). Additionally, we assessed a large cohort including both Latin American and US participants using the FRS, a well-validated, widely used, and easily implementable measure of cardiovascular risk (40). The FRS is particularly suitable for studies in Latin American populations where harmonization across diverse sites is essential. Its inclusion of age, blood pressure, cholesterol, smoking, and diabetes aligns closely with known contributors to allostatic load and interoceptive dysfunction (14-17). Moreover, FRS has been applied across multiple global and LMIC settings (56-59), facilitating comparability and enabling integration with existing epidemiological data. This makes it a pragmatic and theoretically grounded tool for examining how cardiovascular burden affects the allostatic-interoceptive brain network in underserved populations. This cross-cultural approach provides much needed insights into underrepresented populations in dementia research. Recent evidence has highlighted greater structural inequalities as well as accelerated brain aging in dementia in Latin America compared to other parts of the world (68, 80, 81), combined with increased cardiovascular risk in this region (37-39). Although speculative, this work suggests that increased prevalence of cardiovascular risk factors and increased prevalence of dementia in Latin America (37-39, 82) may be driven by allostatic overload and may converge within the AIN. Finally, our multimodal neuroimaging approach allowed for a thorough examination of gray matter volume and functional connectivity of the AIN in dementia syndromes, offering a novel perspective on whole-body health in neurodegeneration.

The current study has some limitations that call for further research. First, our cross-sectional design limits any direct causal interpretations between cardiovascular risk factors and neurodegenerative processes. Longitudinal studies are necessary to confirm causality between cardiovascular risk and structural and functional disruptions within the AIN. In addition, whether addressing cardiovascular risk factors in routine clinical practice in people with dementia has an impact on dementia prognosis warrants attention. Next, the cardiovascular measure we used, namely the Framingham's Risk Score, was limited to non-laboratory measures as laboratory measures were not available across research centers. Although previous evidence suggest non-laboratory measures these are comparable with laboratory measures in measuring cardiovascular risk (56-59), other biomarkers associated with cardiometabolic risk and/or allostatic load (e.g., cholesterol, cortisol), and other relevant physical measures such as waist-to-hip ratio, or key lifestyle factors, such as physical inactivity, nutrition, life-time cigarette burden, and alcohol consumption measures were not measured. Future research is needed to determine how these factors may influence neurodegeneration, potentially via epigenetic mechanisms (83-85). In addition, demographic differences precluded comparisons between AD and FTLD, and a small portion of AD cases were excluded due to older age. Therefore, it is currently unknown whether differences in cardiovascular risk profiles between these dementia syndromes exist, as well as during different stages of dementia, and warrants further consideration. Finally, we did not measure genetic mutations in this study. Over two-thirds FTLD cases are considered to be "sporadic", with no currently known genetic cause (86) and research suggests that cardiovascular risk factors predict the likelihood of AD beyond genetic factors alone (5). A recent study also reported greater prevalence of cardiovascular disease in sporadic than genetic FTD (87). The contribution of cardiovascular risk factors could be more pronounced in "sporadic" FTLD and

AD due to prolonged allostatic overload (6, 7, 13, 18). Future research comparing genetic vs sporadic cohorts will be useful to shed light on this topic.

In conclusion, the current study evidenced substantial associations between cardiovascular health and AIN integrity in dementia. This work aligns with predictive coding theories (6-13), highlighting the role of cumulative cardiovascular stress on allostatic interoception networks vulnerable to dementia pathology. The management of cardiovascular risk factors could represent a key intervention strategy for dementia syndromes, potentially by reducing allostatic load on the AIN. Future work is needed to uncover longitudinal effects of cardiovascular risk on dementia and to determine if cardiovascular risk factors exacerbate neurodegenerative processes, together with clinical consideration of cardiovascular health in dementia diagnosis to minimize disease burden and improve patient outcomes.

5 Acknowledgements

We would like to thank the participants and their families for their time and dedication to our research.

5.1 Fundings sources

JLH and JM are supported by postdoctoral fellowships granted by the multi-partner consortium to expand dementia research in Latin America (ReDLat). JM is supported by a GBBHI fellowship 2024. OC is supported by grants from ISCIII: CP21/00097, P20/00012, PI24/00326, GBHI fellowship 2024. CDA is supported by ANID/FONDECYT Regular 1210622, ANID/PIA/ANILLOS ACT210096, Alzheimer's Association (AARGD-24- 1310017) and ANID/FOVI240065. AI is supported by grants from CONICET; ANID/FONDECYT Regular (1210195 and 1210176 and 1220995); ANID/FONDAP/15150012; ANID/PIA/ANILLOS ACT210096; FONDEF ID20I10152, ID22I10029; ANID/FONDAP 15150012; Takeda CW2680521 and the MULTI-PARTNER CONSORTIUM TO EXPAND DEMENTIA RESEARCH IN LATIN AMERICA [ReDLat, supported by Fogarty International Center (FIC), National Institutes of Health, National Institutes of Aging (R01 AG057234, R01 AG075775, R01 AG021051, R01 AG083799, CARDS-NIH), Alzheimer's Association (SG-20–725707), Rainwater Charitable Foundation – The Bluefield project to cure FTD, and Global Brain Health Institute)].

5.2 Declarations of interest

The authors have no competing interests to declare.

5.3 CreDiT Statement

All authors read and approved the final version of this manuscript. **JLH**, **JM**, and **AI** accessed and verified the underlying data supporting the findings in this manuscript. **JLH**:

Conceptualization; Investigation; Methodology; Formal analysis; Writing – Original Draft, Visualization; **JM**: Conceptualization; Methodology; Formal analysis; Visualization; **RGG**: Data Curation; Methodology, Formal analysis; Writing – review and editing; **FA**: Software, Writing – review and editing; **CA**: Writing – review and editing; **OW**: Visualization; Writing – review and editing; **DSGR**: Data Curation; Writing – review and editing; **PB**: Data Curation; Writing – review and editing; **VM**: Writing – review and editing; **CGC**: Writing – review and editing; **AMCL**: Writing – review and editing; **HH**: Software, Writing – review and editing; **OC**: Writing – review and editing; **KH**: Writing – review and editing; **PL**: Writing – review and editing; **MIB**: Writing – review and editing; **MAB**: Writing – review and editing; J**FC**: Writing – review and editing; **NC**: Writing – review and editing; **HSG**: Writing – review and editing; **AMG**: Writing – review and editing; **MEG**: Writing – review and editing; **JAAF**: Writing – review and editing; **MM**: Data curation, Writing – review and editing; **DLM**: Writing – review and editing; **BM**: Writing – review and editing; **MOO**: Writing – review and editing; **SDPE**: Writing – review and editing; **KLP**: Writing – review and editing; **EPFR**: Writing – review and editing; **PR**: Writing – review and editing; **AS**: Writing – review and editing; **ALS**: Writing – review and editing; **LTT**: Writing – review and editing; **VV**: Writing – review and editing; **JSY**: Writing – review and editing; **AI**: Conceptualization; Methodology; Resources; Project administration; Funding acquisition; Writing – Original Draft.

References

1. Livingston G, Huntley J, Liu KY, Costafreda SG, Selbæk G, Alladi S, et al. Dementia prevention, intervention, and care: 2024 report of the Lancet standing Commission. The Lancet. 2024;404(10452):572-628.
2. Hu H-Y, Ou Y-N, Shen X-N, Qu Y, Ma Y-H, Wang Z-T, et al. White matter hyperintensities and risks of cognitive impairment and dementia: a systematic review and meta-analysis of 36 prospective studies. Neuroscience & Biobehavioral Reviews. 2021;120:16-27.
3. Ibanez A, Zimmer ER. Time to synergize mental health with brain health. Nature Mental Health. 2023;1(7):441-3.
4. Ibanez A, Kringelbach ML, Deco G. A synergetic turn in cognitive neuroscience of brain diseases. Trends in Cognitive Sciences. 2024.
5. Tai XY, Veldsman M, Lyall DM, Littlejohns TJ, Langa KM, Husain M, et al. Cardiometabolic multimorbidity, genetic risk, and dementia: a prospective cohort study. The Lancet Healthy Longevity. 2022;3(6):e428-e36.
6. Ibanez A, Northoff G. Intrinsic timescales and predictive allostatic interoception in brain health and disease. Neuroscience & Biobehavioral Reviews. 2023:105510.
7. Migeot JA, Duran-Aniotz CA, Signorelli CM, Piguet O, Ibáñez A. A predictive coding framework of allostatic–interoceptive overload in frontotemporal dementia. Trends in Neurosciences. 2022.
8. Kleckner IR, Zhang J, Touroutoglou A, Chanes L, Xia C, Simmons WK, et al. Evidence for a large-scale brain system supporting allostasis and interoception in humans. Nature human behaviour. 2017;1(5):1-14.
9. Chen WG, Schloesser D, Arensdorf AM, Simmons JM, Cui C, Valentino R, et al. The emerging science of interoception: sensing, integrating, interpreting, and regulating signals within the self. Trends in neurosciences. 2021;44(1):3-16.
10. Berntson GG, Khalsa SS. Neural circuits of interoception. Trends in neurosciences. 2021;44(1):17-28.
11. Sterling P. Allostasis: a model of predictive regulation. Physiology & behavior. 2012;106(1):5-15.
12. Hazelton JL, Ibanez A, Kumfor F. Interoception in health and disease: theoretical and methodological considerations. Handbook of the Behavior and Psychology of Disease: Springer; 2025. p. 1-18.
13. Franco-O'Byrne D, Santamaría-García H, Migeot J, Ibáñez A. Emerging Theories of Allostatic-Interoceptive Overload in Neurodegeneration. Springer; 2024.
14. Bonaz B, Lane RD, Oshinsky ML, Kenny PJ, Sinha R, Mayer EA, et al. Diseases, disorders, and comorbidities of interoception. Trends in neurosciences. 2021;44(1):39-51.
15. McEwen BS. Allostasis and allostatic load: implications for neuropsychopharmacology. Stress and the Brain. 2013:2-18.
16. Guidi J, Lucente M, Sonino N, Fava GA. Allostatic load and its impact on health: a systematic review. Psychotherapy and psychosomatics. 2021;90(1):11-27.
17. Seeman TE, Singer BH, Rowe JW, Horwitz RI, McEwen BS. Price of adaptation—allostatic load and its health consequences: MacArthur studies of successful aging. Archives of internal medicine. 1997;157(19):2259-68.

18. Hazelton JL, Carneiro F, Maito M, Richter F, Legaz A, Altschuler F, et al. Neuroimaging meta-analyses reveal convergence of interoception, emotion, and social cognition across neurodegenerative diseases. Biological Psychiatry. 2024.
19. Hazelton JL, Fittipaldi S, Fraile-Vazquez M, Sourty M, Legaz A, Hudson AL, et al. Thinking versus feeling: How interoception and cognition influence emotion recognition in behavioural-variant frontotemporal dementia, Alzheimer's disease, and Parkinson's disease. Cortex: A Journal Devoted to the Study of the Nervous System and Behavior. 2023;163:66-79.
20. Hazelton JL, Devenney E, Ahmed R, Burrell J, Hwang Y, Piguet O, et al. Hemispheric contributions toward interoception and emotion recognition in left-vs right-semantic dementia. Neuropsychologia. 2023;188:108628.
21. Birba A, Santamaría-García H, Prado P, Cruzat J, Ballesteros AS, Legaz A, et al. Allostatic interoceptive overload in frontotemporal dementia. Biological Psychiatry. 2022;92(1):54-67.
22. García-Cordero I, Sedeño L, De La Fuente L, Slachevsky A, Forno G, Klein F, et al. Feeling, learning from and being aware of inner states: interoceptive dimensions in neurodegeneration and stroke. Philosophical Transactions of the Royal Society B: Biological Sciences. 2016;371(1708):1-10.
23. Salamone PC, Legaz A, Sedeño L, Moguilner S, Fraile-Vazquez M, Campo CG, et al. Interoception primes emotional processing: Multimodal evidence from neurodegeneration. Journal of Neuroscience. 2021;41(19):4276-92.
24. Woolley J, Gorno-Tempini M-L, Seeley W, Rankin K, Lee S, Matthews B, et al. Binge eating is associated with right orbitofrontal-insular-striatal atrophy in frontotemporal dementia. Neurology. 2007;69(14):1424-33.
25. Ahmed RM, Irish M, Henning E, Dermody N, Bartley L, Kiernan MC, et al. Assessment of Eating Behavior Disturbance and Associated Neural Networks in Frontotemporal Dementia. JAMA Neurology. 2016;73(3):282-90.
26. Wang P, Zhang H, Wang Y, Zhang M, Zhou Y. Plasma cholesterol in Alzheimer's disease and frontotemporal dementia. Translational neuroscience. 2020;11(1):116-23.
27. Hazelton JL, Della Bella G, Barttfeld P, Dottori M, Gonzalez-Gomez R, Migeot J, et al. Altered spatiotemporal brain dynamics of interoception in behavioural-variant frontotemporal dementia. EBioMedicine. 2025;113.
28. Udeh-Momoh CT, Su B, Evans S, Zheng B, Sindi S, Tzoulaki I, et al. Cortisol, amyloid-β, and reserve predicts Alzheimer's disease progression for cognitively normal older adults. Journal of Alzheimer's Disease. 2019;70(2):553-62.
29. De Felice FG, Gonçalves RA, Ferreira ST. Impaired insulin signalling and allostatic load in Alzheimer disease. Nature Reviews Neuroscience. 2022;23(4):215-30.
30. Adedeji DO, Holleman J, Juster R-P, Udeh-Momoh CT, Kåreholt I, Hagman G, et al. Longitudinal study of Alzheimer's disease biomarkers, allostatic load, and cognition among memory clinic patients. Brain, Behavior, & Immunity-Health. 2023;28:100592.
31. Butterfield DA, Halliwell B. Oxidative stress, dysfunctional glucose metabolism and Alzheimer disease. Nature Reviews Neuroscience. 2019;20(3):148-60.
32. Boots EA, Zhan L, Dion C, Karstens AJ, Peven JC, Ajilore O, et al. Cardiovascular disease risk factors, tract-based structural connectomics, and cognition in older adults. Neuroimage. 2019;196:152-60.

33. Song R, Xu H, Dintica CS, Pan K-Y, Qi X, Buchman AS, et al. Associations between cardiovascular risk, structural brain changes, and cognitive decline. Journal of the American College of Cardiology. 2020;75(20):2525-34.
34. Vriend EM, de Sitter A, Bouwmeester TA, Franco OH, Galenkamp H, van Charante EPM, et al. Cardiovascular Risk Factors Impact Brain Volume and White Matter Hyperintensities: A Multiethnic Cohort Study. Journal of Neuroimaging. 2025;35(3):e70057.
35. Srinivasa RN, Rossetti HC, Gupta MK, Rosenberg RN, Weiner MF, Peshock RM, et al. Cardiovascular risk factors associated with smaller brain volumes in regions identified as early predictors of cognitive decline. Radiology. 2016;278(1):198-204.
36. Wang R, Fratiglioni L, Laveskog A, Kalpouzos G, Ehrenkrona CH, Zhang Y, et al. Do cardiovascular risk factors explain the link between white matter hyperintensities and brain volumes in old age? A population-based study. European journal of neurology. 2014;21(8):1076-82.
37. Urina-Jassir M, Jaimes-Reyes MA, Martinez-Vernaza S, Urina-Triana M. The need for creating a unified knowledge of cardiovascular diseases in Latin America. SciELO Brasil; 2022. p. I-II.
38. Shaw PM, Chandra V, Escobar GA, Robbins N, Rowe V, Macsata R. Controversies and evidence for cardiovascular disease in the diverse Hispanic population. Journal of vascular surgery. 2018;67(3):960-9.
39. Gomez S, Blumer V, Rodriguez F. Unique cardiovascular disease risk factors in hispanic individuals. Current Cardiovascular Risk Reports. 2022;16(7):53-61.
40. D'Agostino Sr RB, Vasan RS, Pencina MJ, Wolf PA, Cobain M, Massaro JM, et al. General cardiovascular risk profile for use in primary care: the Framingham Heart Study. Circulation. 2008;117(6):743-53.
41. Prado P, Medel V, Gonzalez-Gomez R, Sainz-Ballesteros A, Vidal V, Santamaría-García H, et al. The BrainLat project, a multimodal neuroimaging dataset of neurodegeneration from underrepresented backgrounds. Scientific Data. 2023;10(1):889.
42. Ibanez A, Yokoyama JS, Possin KL, Matallana D, Lopera F, Nitrini R, et al. The multi-partner consortium to expand dementia research in Latin America (ReDLat): driving multicentric research and implementation science. Frontiers in neurology. 2021;12:631722.
43. Gorno-Tempini ML, Hillis AE, Weintraub S, Kertesz A, Mendez M, Cappa SF, et al. Classification of primary progressive aphasia and its variants. Neurology. 2011;76(11):1006-14.
44. Rascovsky K, Hodges JR, Knopman D, Mendez MF, Kramer JH, Neuhaus J, et al. Sensitivity of revised diagnostic criteria for the behavioural variant of frontotemporal dementia. Brain. 2011;134(9):2456-77.
45. Armstrong MJ, Litvan I, Lang AE, Bak TH, Bhatia KP, Borroni B, et al. Criteria for the diagnosis of corticobasal degeneration. Neurology. 2013;80(5):496-503.
46. Strong MJ, Abrahams S, Goldstein LH, Woolley S, Mclaughlin P, Snowden J, et al. Amyotrophic lateral sclerosis-frontotemporal spectrum disorder (ALS-FTSD): Revised diagnostic criteria. Amyotrophic lateral sclerosis and frontotemporal degeneration. 2017;18(3-4):153-74.
47. Höglinger GU, Respondek G, Stamelou M, Kurz C, Josephs KA, Lang AE, et al. Clinical diagnosis of progressive supranuclear palsy: the movement disorder society criteria. Movement disorders. 2017;32(6):853-64.
48. McKhann GM, Knopman DS, Chertkow H, Hyman BT, Jack Jr CR, Kawas CH, et al. The diagnosis of dementia due to Alzheimer's disease: recommendations from the National

Institute on Aging-Alzheimer's Association workgroups on diagnostic guidelines for Alzheimer's disease. Alzheimer's & dementia. 2011;7(3):263-9.
49. Crutch SJ, Schott JM, Rabinovici GD, Murray M, Snowden JS, van der Flier WM, et al. Consensus classification of posterior cortical atrophy. Alzheimer's & Dementia. 2017;13(8):870-84.
50. Blennerhassett R, Lillo P, Halliday GM, Hodges JR, Kril JJ. Distribution of pathology in frontal variant Alzheimer's disease. Journal of Alzheimer's Disease. 2014;39(1):63-70.
51. Gonzalez-Gomez R, Legaz A, Moguilner S, Cruzat J, Hernández H, Baez S, et al. Educational disparities in brain health and dementia across Latin America and the United States. Alzheimer's & Dementia. 2024.
52. Tombaugh TN, McIntyre NJ. The mini-mental state examination: a comprehensive review. Journal of the American Geriatrics Society. 1992;40(9):922-35.
53. Stuart EA, King G, Imai K, Ho D. MatchIt: nonparametric preprocessing for parametric causal inference. Journal of statistical software. 2011.
54. Morris JC. The Clinical Dementia Rating (CDR) current version and scoring rules. Neurology. 1993;43(11):2412--a.
55. Mioshi E, Flanagan E, Knopman D. Detecting clinical change with the CDR-FTLD: differences between FTLD and AD dementia. International journal of geriatric psychiatry. 2017;32(9):977-82.
56. Alemu YM, Alemu SM, Bagheri N, Wangdi K, Chateau D. Discrimination and calibration performances of non-laboratory-based and laboratory-based cardiovascular risk predictions: a systematic review. Open Heart. 2025;12(1).
57. Dehghan A, Ahmadnia Motlagh S, Khezri R, Rezaei F, Aune D. A comparison of laboratory-based and office-based Framingham risk scores to predict 10-year risk of cardiovascular diseases: a population-based study. Journal of Translational Medicine. 2023;21(1):687.
58. Pandya A, Weinstein MC, Gaziano TA. A comparative assessment of non-laboratory-based versus commonly used laboratory-based cardiovascular disease risk scores in the NHANES III population. PloS one. 2011;6(5):e20416.
59. Rezaei F, Seif M, Gandomkar A, Fattahi MR, Hasanzadeh J. Agreement between laboratory-based and non-laboratory-based Framingham risk score in Southern Iran. Scientific reports. 2021;11(1):10767.
60. Van Buuren S, Groothuis-Oudshoorn K. mice: Multivariate imputation by chained equations in R. Journal of statistical software. 2011;45:1-67.
61. Nichols TE, Das S, Eickhoff SB, Evans AC, Glatard T, Hanke M, et al. Best practices in data analysis and sharing in neuroimaging using MRI. Nature neuroscience. 2017;20(3):299-303.
62. Poldrack RA, Baker CI, Durnez J, Gorgolewski KJ, Matthews PM, Munafò MR, et al. Scanning the horizon: towards transparent and reproducible neuroimaging research. Nature reviews neuroscience. 2017;18(2):115-26.
63. McKinney W, van der Walt S, Millman J. Proceedings of the 9th Python in Science Conference. Austin, Texas; 2010.
64. Seabold S, Perktold J. Statsmodels: econometric and statistical modeling with python. SciPy. 2010;7:1.
65. Brett M, Anton J-L, Valabregue R, Poline J-B. Region of interest analysis using the MarsBar toolbox for SPM 99. Neuroimage. 2002;16(2):S497.

66. Rolls ET, Joliot M, Tzourio-Mazoyer N. Implementation of a new parcellation of the orbitofrontal cortex in the automated anatomical labeling atlas. NeuroImage. 2015;122:1-5.
67. Donnelly-Kehoe PA, Pascariello GO, García AM, Hodges JR, Miller B, Rosen H, et al. Robust automated computational approach for classifying frontotemporal neurodegeneration: multimodal/multicenter neuroimaging. Alzheimer's & Dementia: Diagnosis, Assessment & Disease Monitoring. 2019;11(1):588-98.
68. Legaz A, Altschuler F, Gonzalez-Gomez R, Hernández H, Baez S, Migeot J, et al. Structural inequality linked to brain volume and network dynamics in aging and dementia across the Americas. Nature aging. 2025;5(2):259-74.
69. Legaz A, Abrevaya S, Dottori M, González Campo C, Birba A, Martorell Caro M, et al. Multimodal mechanisms of human socially reinforced learning across neurodegenerative diseases. Brain. 2022;145(3):1052-68.
70. Fittipaldi S, Legaz A, Maito M, Hernandez H, Altschuler F, Canziani V, et al. Heterogeneous factors influence social cognition across diverse settings in brain health and age-related diseases. Nature Mental Health. 2024;2(1):63-75.
71. Penny WD, Friston KJ, Ashburner JT, Kiebel SJ, Nichols TE. Statistical parametric mapping: the analysis of functional brain images: Elsevier; 2011.
72. Nieto-Castanon A. Handbook of functional connectivity magnetic resonance imaging methods in CONN: Hilbert Press; 2020.
73. Jafri MJ, Pearlson GD, Stevens M, Calhoun VD. A method for functional network connectivity among spatially independent resting-state components in schizophrenia. Neuroimage. 2008;39(4):1666-81.
74. Benjamini Y, Hochberg Y. Controlling the false discovery rate: a practical and powerful approach to multiple testing. Journal of the Royal statistical society: series B (Methodological). 1995;57(1):289-300.
75. Abrol A, Fu Z, Salman M, Silva R, Du Y, Plis S, et al. Deep learning encodes robust discriminative neuroimaging representations to outperform standard machine learning. Nature communications. 2021;12(1):353.
76. Koten JW, Manner H, Pernet C, Schüppen A, Szücs D, Wood G, et al. When most fMRI connectivity cannot be detected: Insights from time course reliability. Plos one. 2024;19(12):e0299753.
77. Prado P, Medel V, Ibanez A. BrainLat-dataset. Synapse2023.
78. Biessels GJ, Reagan LP. Hippocampal insulin resistance and cognitive dysfunction. Nature Reviews Neuroscience. 2015;16(11):660-71.
79. Nijskens C, Henstra M, Rhodius-Meester H, Yasar S, van Poelgeest E, Peters M, et al. Cardiovascular risk management in persons with dementia. Journal of Alzheimer's Disease. 2023;93(3):879-89.
80. Moguilner S, Baez S, Hernandez H, Migeot J, Legaz A, Gonzalez-Gomez R, et al. Brain clocks capture diversity and disparities in aging and dementia across geographically diverse populations. Nature medicine. 2024:1-12.
81. Baez S, Hernandez H, Moguilner S, Cuadros J, Santamaria-Garcia H, Medel V, et al. Structural inequality and temporal brain dynamics across diverse samples. Clinical and Translational Medicine. 2024;14(10):e70032.
82. Parra MA, Baez S, Allegri R, Nitrini R, Lopera F, Slachevsky A, et al. Dementia in Latin America: assessing the present and envisioning the future. Neurology. 2018;90(5):222-31.

83. Koulouri A, Zannas AS. Epigenetics as a link between environmental factors and dementia risk. Journal of Alzheimer's Disease Reports. 2024;8(1):957-65.
84. Bui H, Keshawarz A, Wang M, Lee M, Ratliff SM, Lin L, et al. Association analysis between an epigenetic alcohol risk score and blood pressure. Clinical Epigenetics. 2024;16(1):1-12.
85. Tripathi A, Pandey VK, Sharma G, Sharma AR, Taufeeq A, Jha AK, et al. Genomic Insights into Dementia: Precision Medicine and the Impact of Gene-Environment Interaction. Aging and Disease. 2024;15(5):2113.
86. Heuer HW, Wang P, Rascovsky K, Wolf A, Appleby B, Bove J, et al. Comparison of sporadic and familial behavioral variant frontotemporal dementia (FTD) in a North American cohort. Alzheimer's & Dementia. 2020;16(1):60-70.
87. Soppela H, Katisko K, Gadola Y, Krüger J, Hartikainen P, Alberici A, et al. Modifiable potential risk factors in familial and sporadic frontotemporal dementia. Annals of Clinical and Translational Neurology. 2022;9(8):1195-205.

Figure captions

Figure 1. Experimental workflow. A) Sample characterization per country. Color bars indicate the number of participants. Circle plots represent the proportion of participants in each group. B) Assessment protocol. All participants underwent a clinical examination and had an MRI scan. The Framingham Risk Score (FRS) was calculated based on established non-laboratory measures, considering Age, Sex, Presence of Diabetes, Presence of Hypertension, Systolic blood pressure, Body mass index (BMI), and current smoking status. MRI measures included structural T1 MRI and resting state functional MRI (rsFMRI). C). Allostatic interoceptive network (AIN) regions investigated in the neuroimaging analyses. D) Brain-cardiovascular associations using the FRS were investigated in the AIN using structural voxel-based morphometry and functional connectivity analyses.

Figure 2. Brain volume of the allostatic interoceptive network and cardiovascular risk in dementia. Reduced structural integrity associated with increased cardiovascular risk in A) FTLD syndromes and B) in AD syndromes. Whole brain plots display VBM results with TFCE values shown within predefined regions, with FDR $p<.05$. Scatterplots show GM volumes within predefined regions associated with cardiovascular risk scores. Spider plots display Pearson *r*-values for correlations between each ROI and FRS score. Abbreviations: AMYG: Amygdala; CING: Cingulate; HIPP: Hippocampus; INS: Insula; ORB: Orbitofrontal cortex; THAL: Thalamus; FTLD: Frontotemporal Lobar Degeneration; AD: Alzheimer's disease.

Figure 3. Reduced grey matter integrity associated with increased cardiovascular risk in A) FTLD vs AD, and B) AD vs FTLD. Whole brain plots display VBM results with TFCE values shown in predefined regions, with FDR $p<.05$ using a 50 contiguous voxel threshold.

Figure 4. Allostatic interoceptive network functionality and cardiovascular risk in dementia. Reduced functional connectivity associated with increased cardiovascular risk in A) FTLD syndromes; and B) AD syndromes. In each panel, ROI-to-ROI connectivity maps are shown. Connectome rings show the strength of connectivity between each ROI, with color bars representing the connectivity strength using t-values. Radial plots show the number of connections of each ROI to different regions, with color bars representing the maximum number of ROI connections. Abbreviations: CINGmid: Middle cingulate cortex; CINGpost: Posterior cingulate cortex; HIPP: Hippocampus; INS: Insula; ORBinf: Orbitofrontal cortex (inferior); ORBmed: Orbitofrontal cortex (medial); ORBmid: Orbitofrontal cortex (middle); ORBsup: Orbitofrontal cortex (superior); ParaHIPP: Parahippocampal gyrus; THAL: Thalamus.

Supplementary materials

Supplementary methods

Demographics, cognitive assessment, and cardiovascular risk in FTLD and AD subtypes

Demographics, cognitive assessment, and cardiovascular risk was compared between FTD subtypes and controls (Supplementary Table 1) and AD subtypes and controls (Supplementary Table 2).

FTD subtypes

In brief, no significant differences were found for age or sex in FTD subtypes and controls. FTD mixed (corticobasal syndrome, progressive supranuclear palsy and FTD with motor neuron disease) had fewer years of education compared to bvFTD and controls. All FTD subtypes showed worse cognitive performance than controls, and nfvPPA had lower cognitive scores than bvFTD. bvFTD and svPPA had a more severe dementia stage than nfvPPA, and bvFTD had a more severe disease stage than FTD-mixed. Cardiovascular risk scores were not significantly different between FTD subtypes and controls.

AD subtypes

In AD subtypes, PCA were significantly younger than ADa. Further, fv-AD and lvPPA had the reversed pattern of expected frequencies for sex. ADa had fewer years of education compared to lvPPA. All AD subtypes showed worse cognitive performance than controls. All AD-subtype patients were at a mild-to-moderate disease stage on average. Notable differences in disease stages were that PCA patients had a more severe disease stage than lvPPA. Finally, PCA patients had a lower cardiovascular risk score compared to ADa patients.

Supplementary Table 1. Demographics in FTD subtypes compared to controls.

	CN	bvFTD	nfvPPA	svPPA	FTD mixed [a]	Statistic	*p*	Post hoc
	(n = 304)	(n = 189)	(n = 38)	(n = 52)	(n = 25)			
Age	64.78 ± 8.60	64.49 ± 7.99	67.5 ± 7.43	66.27 ±7.54	67.76 ± 7.25	2.11	0.078	ns
Sex (M:F)	166:138	113:76	16:22	23:29	14:11	11.48	0.175	ns
Education	14.56 ± 5.46	14.68 ± 4.14	13.68 ± 4.83	14.31 ± 4.59	11.32 ± 4.54	2.87	0.022	FTD mixed < bvFTD & CN
MMSE	28.14 ± 3.00	22.11 ± 6.43	19.46 ± 8.97	20.12 ± 4.91	22.96 ± 4.24	69.71	<.001	All < CN; nfvPPA < bvFTD
CDR	-	9.38 ± 3.79	6.17 ± 4.97	8.62 ± 2.98	6.96 ± 3.51	9.28	<.001	nfvPPA < svPPA & bvFTD FTD mixed < bvFTD
FRS	13.67 ± 3.99	13.66 ± 3.95	14.29 ± 3.97	13.71 ± 3.27	14.36 ± 4.07	0.39	0.818	ns

Note. Post hoc tests were conducted using Tukey HSD, FWE p <.05; [a] FTD mixed = 9 CBS, 12 PSP, 2 FTD-MND. Abbreviations: bvFTD = behavioral-variant frontotemporal dementia; nfvPPA = nonfluent-variant of primary progressive aphasia; svPPA = semantic-variant primary progressive aphasia; FTD = frontotemporal dementia; CBS = Corticobasal syndrome; CN = controls; PSP = Progressive supranuclear palsy' FTD-MND = FTD with motor neuron disease; ns = not significant.

Supplementary Table 2. Demographics in AD subtypes compared to controls.

	CN	ADa	Atypical AD			Statistic	*p*	Post hoc
			lvPPA	PCA	fv-AD			
	(n = 432)	(n = 375)	(n = 24)	(n = 13)	(n =17)			
Age	67.68 ± 7.25	69.07 ± 7.42	66.08 ± 6.59	62.54 ± 7.24	65.41 ± 8.28	4.88	<.001	PCA < ADa
Sex (M:F)	113:241	145:287	14:10	5:8	11:6	14.33	0.014	fv-AD & lvPPA only [a]
Education	13.27 ± 5.92	12.47 ± 4.93	15.75 ± 4.11	14.69 ± 4.55	14.88 ± 3.77	3.09	0.009	ADa < lvPPA
MMSE	27.50 ± 3.36	20.50 ± 5.18	18.33 ± 8.23	16.83 ± 4.55	18.35 ± 6.53	123.39	<.001	All patients < CN
CDR	-	5.79 ± 2.81	5.0 ± 2.73	7.77 ± 3.15	5.32 ± 1.86	2.65	0.032	lvPPA < PCA
FRS	14.54 ± 3.90	15.23 ± 4.18	14.29 ± 3.21	11.77 ± 3.15	14.24 ± 3.60	2.80	0.016	PCA < ADa

Note. Post hoc tests were conducted using Tukey HSD, FWE $p < .05$; [a] For fv-AD & lvPPA, the actual sex frequencies were reversed compared to the expected sex frequencies. Abbreviations: ADa = Alzheimer's Disease amnestic; lvPPA = logopenic-variant of primary progressive aphasia; PCA = posterior cortical atrophy; fv-AD = frontal-variant of Alzheimer's disease.

Measures

Framingham's Risk Score calculation

The Framingham's Risk Score (1) was calculated based on non-laboratory measures. Scoring is presented in Supplementary Table 3. Body mass index (BMI) was measured as a ratio between weight (kg) and height (cm) squared. Hypertension status (based on clinical reports and medication use) was taken into account when scoring systolic blood pressure. Smoking status related to the participant's self-report of smoking. Diabetes status was based on clinical reports and medication use.

Supplementary Table 3. Framingham's risk score calculations based on non-laboratory measures in females and males.

Points	**Age**	**BMI**	**SBP (not treated)**	**SBP (treated)**	**Smoker**	**Diabetes**
Women						
-3			<120			
-1				<120		
0	30-34	<25	120-129		No	No
1		25-29.9	130-139			
2	35-39	>=30		120-129		
3			140-149	130-139		
4			150-159		Yes	
5	40-44		160+	140-149		Yes
6	45-49			150-159		
8	50-54			160+		
10	55-59					
11	60-64					
12	65-69					
14	70-74					
15	75+					
Men						
-2						
0	30-34	<25	120-129	<120	No	No
1		25-29.9	130-139			
2	35-39	>=30	140-149	120-129		
3			160+	130-139		Yes
4				140-159	Yes	
5	40-44			160+		
7	45-49					
8	50-54					
10	55-59					
11	60-64					
13	65-69					
14	70-74					
15	75+					

Note. Abbreviations: BMI = Body Mass Index; SBP = Systolic Blood Pressure

Resting state functional connectivity analysis

Preprocessing. Functional data were smoothed using spatial convolution with a Gaussian kernel of 6 mm full width half maximum (FWHM).

Denoising. In addition, functional data were denoised using a standard denoising pipeline (2) including the regression of potential confounding effects characterized by white matter timeseries (5 CompCor noise components), CSF timeseries (5 CompCor noise components), motion parameters and their first order derivatives (12 factors)(3), outlier scans (below 526 factors)(4), session and task effects and their first order derivatives (2 factors), and linear trends (2 factors) within each functional run, followed by bandpass frequency filtering of the BOLD time series (5) between 0.008 Hz and 0.09 Hz. CompCor(6, 7) noise components within white matter and CSF were estimated by computing the average BOLD signal as well as the largest principal components orthogonal to the BOLD average, motion parameters, and outlier scans within each subject's eroded segmentation masks. From the number of noise terms included in this denoising strategy, the effective degrees of freedom of the BOLD signal after denoising were estimated to range from 0 to 107.7 (average 52.3) across all subjects (8).

First-level analysis. ROI-to-ROI connectivity (RRC) matrices were estimated characterizing the functional connectivity between each pair of regions among 116 ROIs (9). Functional connectivity strength was represented by Fisher-transformed bivariate correlation coefficients from a general linear model (weighted-GLM(1)), estimated separately for each pair of ROIs, characterizing the association between their BOLD signal time series. In order to compensate for possible transient magnetization effects at the beginning of each run, individual scans were weighted by a step function convolved with an SPM canonical hemodynamic response function and rectified.

Supplementary Table 4. Structural MRI acquisition protocols.

Scanner	Scanner Model	Sequence name	TR (ms)	TE (ms)	Flip angle (°)	No. slices	Matrix dimensions	Voxel size (mm)
1	GE Signa HDxt 1.5T	SAG T1 3D	6500	2.78	12	106	512 x 623x 106	0.5 x 0.5 x 0.5
2	Philips Achieva 3T	TFE	7620	3.70	8	256	170 x 240 x 240	1 x 1 x 1
3	Philips Ingenia 3T	T1 3D FFE	7780	3.60	8	576	355 x 576 x 576	0.5 x 0.4 x 0.4
4	Philips Ingenia Elition X 3T	T1 3D FFE	7780	3.55	8	576	355 x 576 x 576	0.5 x 0.4 x 0.4
5	Siemens Biograph_mMR 3T	MP RAGE	2300	2.9	9	256	176 x 240 x 256	1 x 1 x 1
6	Siemens Magnetom Lumina 3T	MP RAGE	1800	2.13	8	256	192 x 256 x 256	1 x 1 x 1
7	Siemens PrismaFit 3T	MP RAGE	2300	2	9	256	160 x 240 x 256	1 x 1 x 1
8	Siemens Skyra 3T	MP RAGE	1700	2.25	8	224	208 x 224 x 224	1 x 1 x 1
9	Siemens Spectra 3T	MP RAGE	1900	2.42	9	256	176 x 256 x 256	1 x 1 x 1
10	Siemens TrioTim 3T	MP RAGE	2300	2	9	256	160 x 240 x 256	1 x 1 x 1
11	Siemens Verio 3T	MP RAGE	2300	2.9	9	256	176 x 240 x 256	1 x 1 x 1

Supplementary Table 5. Resting-state fMRI protocol information.

Scanner	Scanner Model	TR (ms)	TE (ms)	Voxel size (mm)	No. volumes	Matrix dimension	Flip angle (°)	No. slices	Duration (min)
1	GE Signa HDxt 1.5T	2500	30	3.7 x 3.7 x 5	120	64 x 64	50	33	5
2	Philips Achieva 3T	3000	30	3 x 3 x 3	160	80 x 80	90	40	8
3	Philips Ingenia 3T	4970	30	2.5 x 2.5 x 2.7	121	96 x 96	82	45	10
4	Philips Ingenia Elition X 3T	4970	30	2.5 x 2.5 x 2.7	121	96 x 96	82	45	10
5	Siemens Biograph_mMR 3T	3000	30	3.4 x 3.4 x 3.4	197	64 x 64	90	48	10
6	Siemens Magnetom Lumina 3T	2500	30	2.5 x 2.5 x 2.5	235	94 x 94	94	66	10
7	Siemens PrismaFit 3T	2000	32	2.2 x 2.2 x 2.2	560	96 x 96	45	66	8
8	Siemens Skyra 3T	2660	30	3 x 3 x 3	300	76 x 76	90	46	10
9	Siemens TrioTim 3T	2000	27	2.5 x 2.5 x 3.5	240	92 x 92	80	36	8
10	Siemens Verio 3T	3000	30	3.4 x 3.4 x 3.4	197	64 x 64	90	48	10

Supplementary results

Structural neuroimaging results

Patterns of brain atrophy

Supplementary Table 6. Atrophy patterns in FTLD combined compared to healthy controls.

				MNI				
Peak region	**Association regions**	**Side**	**Size**	**X**	**Y**	**Z**	**t**	**FWE *p***
Hippocampus	Putamen, insula	L	376724	-32	-14	-12	21.30	<.001
Insula	Inferior frontal gyrus	L	-	-36	14	4	21.01	<.001
Insula	Orbitofrontal cortex	L	-	-34	21	-9	20.96	<.001

Note. Whole brain voxelwise, FWE, p <.001, 100 contiguous voxels.

Behavioural-variant frontotemporal dementia (bvFTD)

Supplementary Table 7. Atrophy patterns in bvFTD compared to healthy controls.

				MNI				
Peak region	**Association regions**	**Side**	**Size**	**X**	**Y**	**Z**	**t**	***p**
Rectus	Orbitofrontal cortex (medial), insula	L	59428	-2	38	-16	5.24	<0.001
Orbitofrontal cortex	Insula, rectus,	R	-	8	45	-12	4.96	<0.001
Middle cingulate cortex	Paracentral lobule	L	-	-3	-26	40	4.93	<0.001
Postcentral gyrus	Parietal cortex (inferior and superior)	R	1212	39	-38	56	4.40	<0.001
Parietal cortex (inferior)	Angular gyrus, parietal cortex (superior)	R	-	38	-51	51	3.85	<0.001
Occipital (mid)	Occipital (superior), cuneus	L	477	-28	-86	24	4.04	<0.001
Occipital (mid)	Occipital (superior), cuneus	L	-	-24	-90	15	3.54	<0.001
Postcentral gyrus	Precentral gyrus, supramarginal gyrus	L	814	-52	-12	30	4.00	<0.001
Middle frontal gyrus	Inferior frontal gyrus, superior frontal gyrus	R	620	42	45	14	3.91	<0.001
Middle frontal gyrus	Inferior frontal gyrus, superior frontal gyrus	R	-	40	40	32	3.82	<0.001
Occipital (mid)	Middle temporal gyrus, occipital (superior)	R	210	39	-80	18	3.88	<0.001
Middle temporal gyrus	Superior temporal gyrus, inferior temporal gyrus	R	1272	62	-28	-2	3.86	<0.001
Middle temporal gyrus	Superior temporal gyrus, inferior temporal gyrus	R	-	62	-24	-15	3.76	<0.001
Middle temporal gyrus	Superior temporal gyrus, supramarginal gyrus	R	-	62	-48	12	3.68	<0.001

Precentral gyrus	Postcentral gyrus, superior frontal gyrus	R	167	40	-16	58	3.84	<0.001
Postcentral gyrus	Parietal (inferior), supramarginal gyrus	L	286	-50	-33	50	3.69	<0.001
Precentral gyrus	Frontal inferior operculum	R	236	51	-3	33	3.66	<0.001
Middle temporal gyrus	Occipital (middle and inferior)	L	291	-45	-69	9	3.57	<0.001
Middle temporal gyrus	Inferior temporal gyrus, occipital (inferior)	L	-	-51	-64	-3	3.53	<0.001
Postcentral gyrus	Precentral gyrus, parietal (inferior)	L	171	-34	-22	52	3.57	<0.001
Superior temporal gyrus	Supramarginal gyrus, rolandic operculum	R	261	58	-33	18	3.55	<0.001
Occipital (mid)	Parietal (inferior), occipital (inferior)	L	120	-28	-76	40	3.53	<0.001
Precentral gyrus	Paracentral lobule, Supplementary motor area	R	149	16	-26	69	3.48	<0.001
Occipital	-	R	157	26	-88	27	3.44	<0.001
Cuneus	-	R	-	14	-82	34	3.27	0.001
Occipital	-	R	-	30	-87	16	3.11	0.001

Note. Whole brain voxelwise, *p <.001 uncorrected. 100 contiguous voxels.

Nonfluent variant primary progressive aphasia (nfvPPA)

Supplementary Table 8. Atrophy patterns in nonfluent primary progressive aphasias compared to healthy controls.

				MNI				
Peak region	**Association regions**	**Side**	**Size**	**X**	**Y**	**Z**	**t**	***p**
Postcentral	Precentral gyrus, parietal (inferior)	L	29361	-51	-8	38	5.68	<0.001
Superior temporal gyrus	Heschl's gyrus, rolandic operculum, insula	L	-	-63	-14	9	5.00	<0.001
Superior temporal gyrus	Heschl's gyrus, rolandic operculum, insula	L	-	-50	-10	3	4.84	<0.001
Supplementary motor	Superior frontal gyrus	L	13193	-4	12	51	5.57	<0.001
Precuneus	Calcarine	L	-	-2	-63	22	4.65	<0.001
Middle cingulate cortex	Superior frontal gyrus (medial), anterior cingulate cortex	L	-	-4	24	36	4.56	<0.001
Precentral gyrus	Frontal operculum (inferior)	R	6554	52	-3	33	4.78	<0.001
Rolandic operculum	Heschl's gyrus, insula, superior temporal gyrus	R	-	58	-6	9	4.30	<0.001
Postcentral gyrus	Precentral gyrus, rolandic operculum	R	-	64	0	21	4.27	<0.001
Inferior temporal gyrus	Cerebellum	L	1905	-45	-50	-24	4.30	<0.001
Fusiform	Cerebellum, Occipital (inferior)	L	-	-28	-72	-14	3.77	<0.001
Fusiform	Cerebellum	L	-	-21	-78	-12	3.68	<0.001
Occipital (mid)	Middle temporal gyrus, Occipital (superior)	R	697	42	-81	16	4.14	<0.001
Occipital (mid)	Occipital (superior), cuneus	R	-	28	-86	12	3.28	0.001
Occipital (mid)	Angular gyrus, Middle temporal gyrus	R	-	46	-72	27	3.27	0.001

Middle frontal gyrus	Inferior frontal gyrus, superior frontal gyrus	L	600	-45	54	14	4.08	<0.001
Inferior frontal gyrus	Middle frontal gyrus	L	-	-42	45	2	3.99	<0.001
Fusiform	Lingual gyrus, cerebellum	R	629	26	-80	-14	4.03	<0.001
Lingual gyrus	Cerebellum	R	-	15	-81	-12	3.68	<0.001
Occipital (inferior)	Inferior temporal gyrus, middle temporal gyrus	L	466	-51	-68	-4	3.98	<0.001
Angular gyrus	Superior temporal gyrus, middle temporal gyrus	R	499	57	-57	24	3.94	<0.001
Middle temporal gyrus	Superior temporal gyrus, angular gyrus	R	-	63	-51	10	3.36	<0.001
Middle temporal gyrus	Superior temporal gyrus, angular gyrus	R	-	58	-64	12	3.34	<0.001
Occipital	-	R	431	38	-76	39	3.93	<0.001
Occipital	-	L	471	-27	-86	24	3.88	<0.001
Occipital	-	L	-	-32	-80	21	3.67	<0.001
Occipital	-	L	-	-24	-90	15	3.51	<0.001
Thalamus	-	L	122	-2	4	-2	3.66	<0.001

Note. Whole brain voxelwise, *p <.001 uncorrected. 100 contiguous voxels.

Semantic variant Primary Progressive Aphasia (svPPA)

Supplementary Table 9. Atrophy patterns in the semantic variant of primary progressive aphasia compared to healthy controls.

				MNI				
Peak region	**Association regions**	**Side**	**Size**	**X**	**Y**	**Z**	**t**	***p**
Fusiform	Inferior temporal gyrus, parahippocampal gyrus	L	159034	-33	-9	-39	10.08	<0.001
Temporal pole	Superior temporal gyrus, middle temporal gyrus	L	-	-45	9	-21	9.71	<0.001
Temporal pole	Superior temporal gyrus, middle temporal gyrus	L	-	-46	2	-16	9.65	<0.001
Occipital (mid)	Middle temporal gyrus, occipital (superior)	R	1215	42	-81	18	4.11	<0.001
Occipital (mid)	Middle temporal gyrus, angular gyrus	R	-	51	-80	24	3.72	<0.001
Occipital (mid)	Occipital (superior), cuneus	R	-	26	-84	10	3.71	<0.001
Parietal (superior)	Parietal (inferior), postcentral gyrus	L	936	-30	-52	57	3.97	<0.001
Parietal (inferior)	Angular gyrus, occipital (middle)	L	-	-33	-51	40	3.81	<0.001
Parietal (inferior)	Postcentral gyrus, angular gyrus	L	-	-32	-42	42	3.73	<0.001
Postcentral gyrus	Parietal (inferior and superior)	R	892	40	-36	56	3.89	<0.001
Parietal (inferior)	Supramarginal gyrus, postcentral gyrus	R	-	51	-36	50	3.86	<0.001
Parietal (inferior)	Supramarginal gyrus, parietal (superior)	R	-	56	-45	51	3.53	<0.001
Parietal (superior)	Angular gyrus, parietal (inferior)	R	371	38	-57	54	3.67	<0.001
Angular gyrus	Parietal (superior and inferior)	R	-	32	-62	48	3.59	<0.001

Parietal (inferior)	Angular gyrus, parietal (superior)	R	-	44	-57	48	3.57	<0.001
Postcentral gyrus	Parietal (inferior), supramarginal gyrus	L	158	-51	-33	51	3.53	<0.001
Postcentral gyrus	Precentral, supramarginal gyrus	L	256	-52	-12	30	3.49	<0.001
Postcentral gyrus	Parietal (inferior), supramarginal gyrus	L	-	-50	-15	38	3.31	0.001

Note. Whole brain voxelwise, *p <.001 uncorrected. 100 contiguous voxels.

Corticobasal syndrome, progressive supranuclear palsy, FTD with motor neuron disease (CBS, PSP, FTD-MND)

Supplementary Table 10. Atrophy patterns in FTD-mixed, including corticobasal syndrome, progressive supranuclear palsy and FTD-with motor neuron disease features compared to healthy controls.

				MNI				
Peak region	**Association regions**	**Side**	**Size**	**X**	**Y**	**Z**	**t**	***p**
Cerebellum	Inferior temporal gyrus, fusiform gyrus	L	1999	-46	-51	-30	4.54	<0.001
Cerebellum	-	L	-	-54	-48	-42	4.13	<0.001
Angular gyrus	Parietal (inferior), occipital (middle)	L	901	-33	-52	36	4.24	<0.001
Parietal (superior)	Parietal (inferior), postcentral gyrus	L	-	-30	-50	57	3.33	<0.001
Parietal (inferior)	Postcentral gyrus, parietal (superior)	L	-	-30	-44	46	3.29	0.001
Precuneus	Parietal (superior), paracentral lobule	R	2657	10	-52	57	4.23	<0.001
Paracentral lobule	Precuneus, middle cingulate cortex	L	-	-9	-38	63	4.17	<0.001
Precuneus	Parietal (superior), postcentral gyrus	L	-	-9	-52	66	3.89	<0.001
Postcentral gyrus	Rolandic operculum, precentral gyrus, insula	R	1180	68	2	15	4.15	<0.001
Rolandic operculum	Superior temporal gyrus, Heschl’s gyrus	R	-	66	-6	9	4.07	<0.001
Precentral gyrus	Frontal operculum (inferior), rolandic operculum	R	-	64	12	14	3.54	<0.001

Supplementary Motor	Superior frontal gyrus	R	945	6	-3	66	3.96	<0.001
Supplementary Motor	Superior frontal gyrus	L	-	-4	-2	66	3.79	<0.001
Supplementary Motor	Superior frontal gyrus	L	-	-8	8	72	3.42	<0.001
Middle frontal gyrus	Inferior frontal gyrus, superior frontal gyrus	L	141	-44	56	15	3.76	<0.001
Postcentral gyrus	Precentral gyrus, rolandic operculum, insula	R	168	44	-34	54	3.75	<0.001
Superior frontal gyrus	Middle frontal gyrus	L	336	-24	39	27	3.68	<0.001
Postcentral gyrus	Precentral gyrus, Rolandic operculum	L	555	-51	-14	28	3.67	<0.001
Precentral gyrus	Postcentral gyrus, parietal (inferior)	L	-	-42	-10	40	3.67	<0.001
Postcentral gyrus	Postcentral gyrus, parietal (inferior)	L	-	-36	-24	39	3.27	0.001
Supplementary motor	Paracentral lobule	R	141	2	-22	54	3.52	<0.001
Cerebellum	-	R	130	45	-56	-40	3.47	<0.001
Cerebellum	-	R	-	54	-60	-40	3.19	0.001

Note. Whole brain voxelwise, *p <.001 uncorrected. 100 contiguous voxels.

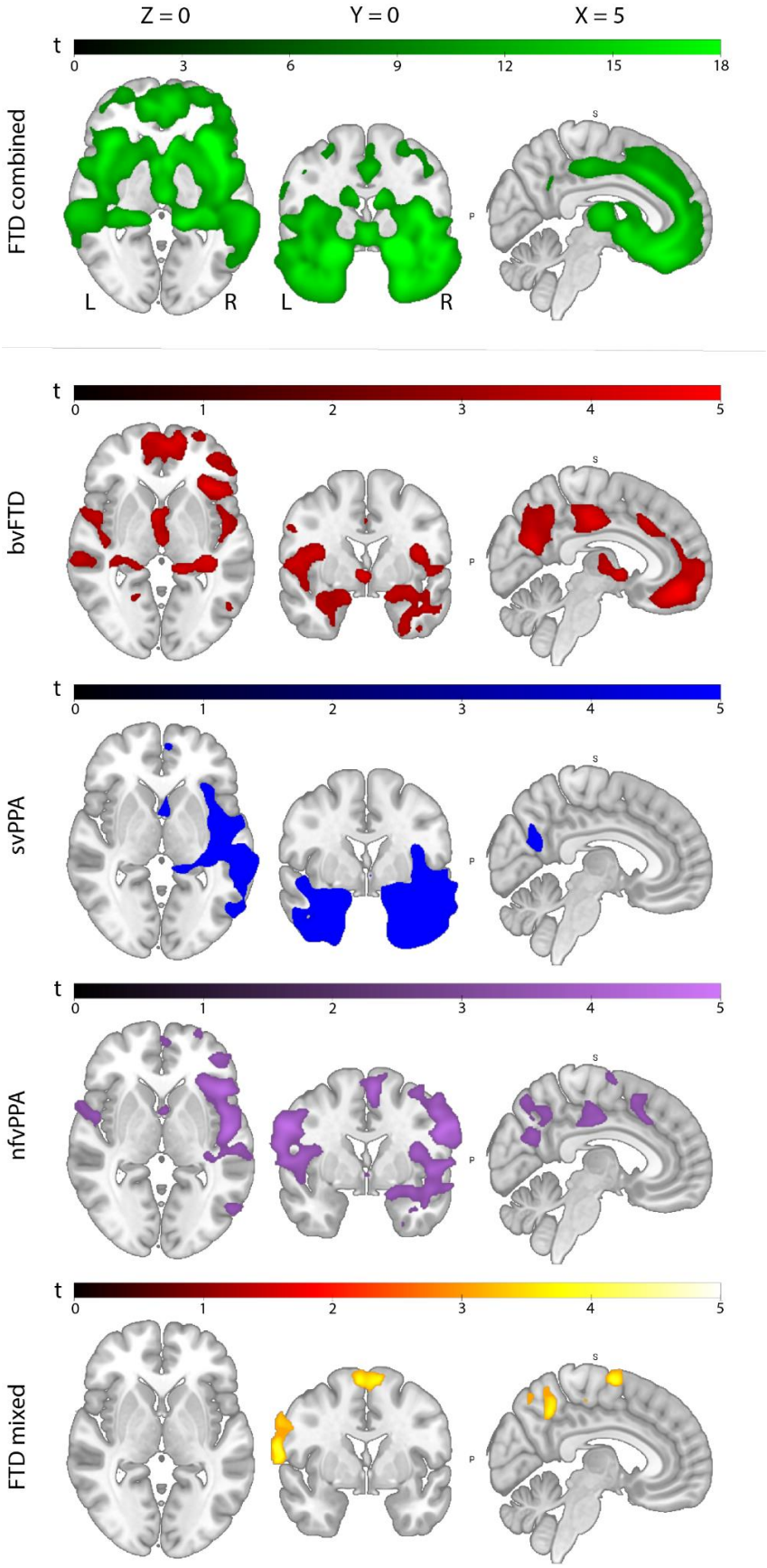

Supplementary Figure 1. Atrophy compared to controls in FTLD vs controls (p-FWE, p<.001), and in subtypes (p-uncorr<0.001).

Alzheimer's disease subtypes

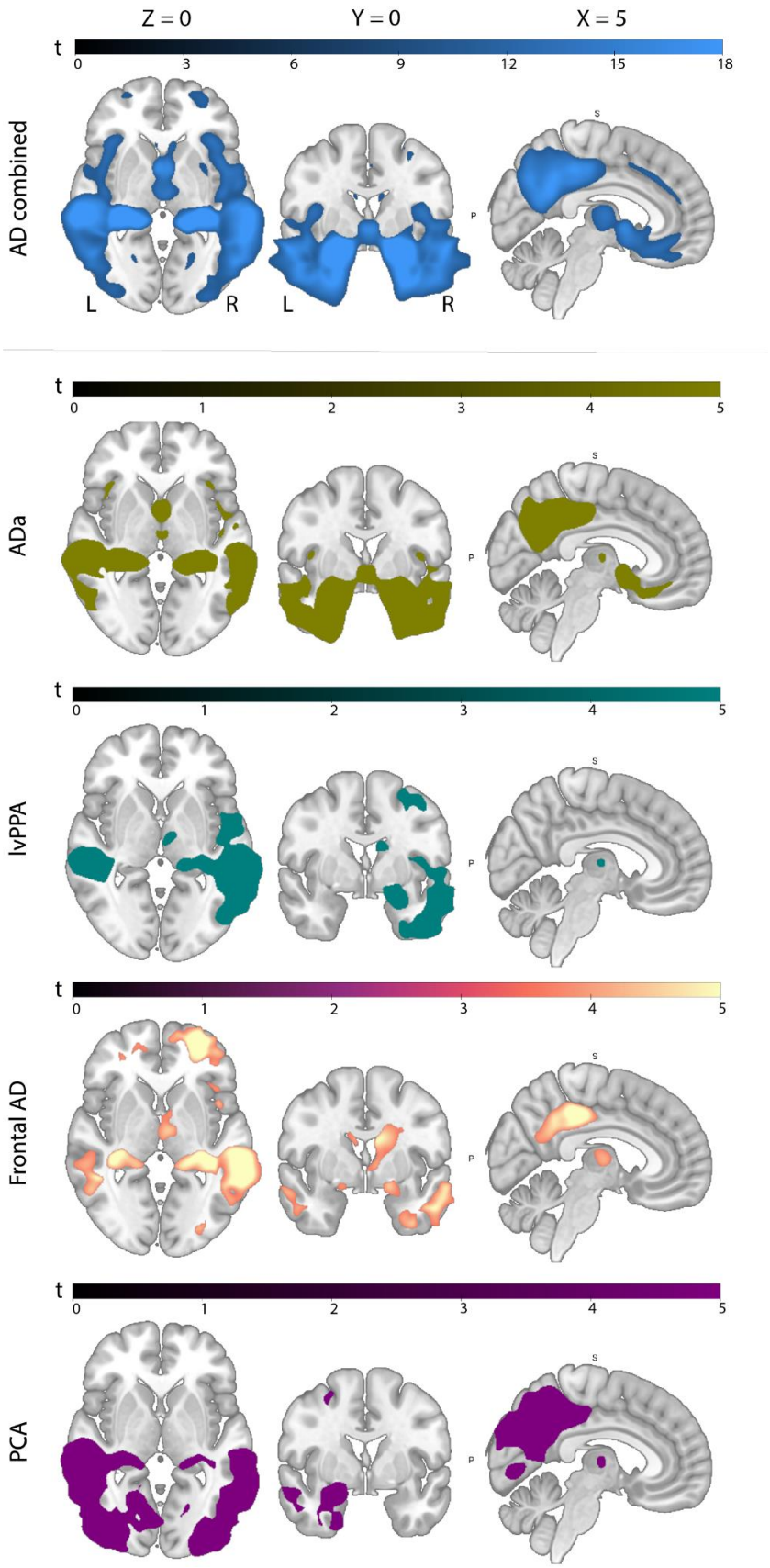

Supplementary Figure 2. Atrophy compared to controls in AD vs controls (p-FWE, p<.001), and in subtypes (p-uncorr<0.001)

Supplementary Table 11. Atrophy patterns in Alzheimer's disease combined compared to healthy controls.

Peak region	Association regions	Side	Size	MNI			t	FDR *p*
				X	Y	Z		
Amygdala	Parahippocampal gyrus, olfactory cortex, temporal pole, superior temporal gyrus, putamen, orbitofrontal cortex (medial and posterior), rectus, hippocampus, insula, thalamus, anterior and posterior cingulate cortex, and precuneous bilaterally	R	43986	21	4	-18	7.65	0.001
Rectus	Orbitofrontal cortex, superior frontal gyrus	L	-	-9	30	-24	7.52	0.001
Amygdala	Olfactory cortex, temporal pole, superior temporal gyrus, Insula, orbitofrontal cortex (medial and posterior), parahippocampal gyrus, putamen, rectus	L	-	-24	4	-18	7.43	0.001
Middle frontal gyrus	Superior frontal gyrus, inferior frontal gyrus, frontal pole	L	168	-44	56	-2	2.35	0.015
Middle frontal gyrus	Orbitofrontal cortex (lateral and anterior), inferior frontal gyrus, superior frontal gyrus, frontal pole	L	-	-42	50	-9	2.34	0.017

Note. All Alzheimer's presentations included (typical and atypical). All clusters are reported at TFCE, FDR-corrected $p < .05$, 50 contiguous voxels threshold. Peak region relates to the coordinates displayed in the table; associate regions are within the cluster. Covariates included group (AD vs control), scanner, and TIV.

Alzheimer's Disease subtypes

Alzheimer's Disease (amnestic)

Supplementary Table 12. Atrophy patterns in Alzheimer's disease with amnestic features (typical AD) compared to healthy controls.

				MNI				
Peak region	**Association regions**	**Side**	**Size**	**X**	**Y**	**Z**	**t**	***p**
Amygdala	**Putamen**	R	678510	27	-9	-14	25.76	<.001
Hippocampus	Amygdala, putamen	L		-27	-10	-14	25.73	<.001
Hippocampus	Parahippocampal gyrus, thalamus	L		-27	-32	-8	23.15	<.001
Cerebellum	-	R	1330	8	-60	-70	4.82	<.001

Note. Whole brain voxelwise, *p <.001 uncorrected. 100 contiguous voxels.

Atypical Alzheimer's Disease

Logopenic-variant of Primary Progressive Aphasia

Supplementary Table 13. Atrophy patterns in logopenic-variant primary progressive aphasia compared to healthy controls.

				MNI				
Peak region	**Association regions**	**Side**	**Size**	**X**	**Y**	**Z**	**t**	***p**
Middle temporal gyrus	Angular gyrus, superior temporal gyrus	L	292468	-58	-58	15	12.02	<0.001
Inferior temporal gyrus	Temporal fusiform, occipital (inferior)	L	-	-51	-52	-18	11.51	<0.001
Middle temporal gyrus	Superior temporal gyrus, Inferior temporal gyrus	L	-	-64	-26	-4	11.39	<0.001
Anterior cingulate cortex	Orbitofrontal cortex (medial), rectus	R	490	16	33	-8	3.80	<0.001
Orbitofrontal cortex	Middle frontal gyrus, orbitofrontal cortex	R	-	28	39	-14	3.51	<0.001
Orbitofrontal cortex	Superior frontal gyrus, Orbitofrontal cortex	R	-	20	48	-9	3.33	<0.001

Note. Whole brain voxelwise, *p <.001 uncorrected. 100 contiguous voxels.

Frontal-variant Alzheimer's Disease

Supplementary Table 14. Atrophy patterns of frontal-variant Alzheimer's Disease compared to healthy controls.

				MNI				
Peak region	**Association regions**	**Side**	**Size**	**X**	**Y**	**Z**	**t**	***p**
Middle frontal gyrus	Superior frontal gyrus, inferior frontal gyrus	L	107452	-32	57	12	7.18	<.001
Middle temporal gyrus	Inferior temporal gyrus, superior temporal gyrus	L	-	-44	-21	-14	7.05	<.001
Middle temporal gyrus	Inferior temporal gyrus, superior temporal gyrus	L	-	-57	-30	-9	6.87	<.001
Insula	Inferior frontal gyrus, inferior frontal operculum	R	177	39	21	3	3.51	<.001
Insula	Inferior frontal operculum, putamen	R	-	38	8	8	3.39	<.001

Note. Whole brain voxelwise, **p* <.001 uncorrected. 100 contiguous voxels.

Posterior cortical atrophy

Supplementary Table 15. Atrophy patterns of posterior cortical atrophy compared to healthy controls.

				MNI				
Peak region	**Association regions**	**Side**	**Size**	**X**	**Y**	**Z**	**t**	***p**
Temporal fusiform	Cerebellum, occipital (inferior)	R	382446	28	-76	-15	12.18	<0.001
Occipital (superior)	Occipital (mid), cuneus	R	-	30	-86	26	10.71	<0.001
Temporal fusiform	Occipital (inferior), lingual	R	-	33	-60	-9	10.68	<0.001

Note. Whole brain voxelwise, *p <.001 uncorrected. 100 contiguous voxels.

Structural correlates associated with cardiovascular risk

Supplementary Table 16. Structural correlates of cardiovascular risk in FTLD.

Peak region	Association regions	Side	Size	MNI			t	FDR *p*
				X	Y	Z		
Insula	Heschl's gyrus, orbitofrontal cortex, middle frontal gyrus, amygdala, hippocampus, parahippocampus, thalamus, posterior cingulate cortex, planum polare, temporal pole	R	8693	45	-15	9	7.14	0.002
Insula	Superior temporal gyrus, rolandic operculum, planum polare	R	-	51	2	-2	5.65	0.002
Hippocampus	Thalamus, parahippocampus	R	-	36	-36	-4	5.54	0.002
Hippocampus	Parahippocampal gyrus, thalamus, amygdala, insula,	L	2634	-21	-42	-8	5.99	0.002
Hippocampus	Parahippocampal gyrus, thalamus, amygdala	L	-	-34	-39	-4	4.96	0.002
Hippocampus	Thalamus, parahippocampal gyrus	L	-	-15	-38	0	4.91	0.002
Mid Cingulate cortex	Anterior cingulate cortex, posterior cingulate cortex, orbitofrontal cortex bilaterally	R	9280	2	-24	46	5.76	0.002
Mid Cingulate cortex	Posterior cingulate cortex, anterior cingulate cortex bilaterally	R	-	6	-16	48	5.54	0.002
Mid Cingulate cortex	Anterior cingulate cortex bilaterally	R	-	2	20	38	5.04	0.002
Insula	Rolandic operculum	L	325	-38	-22	14	4.81	0.002

Insula	Parietal operculum	L	-	-36	-28	20	4.23	0.002
Insula	Heschl's gyrus, planum polare	L	-	-46	-10	4	3.89	0.002
Orbitofrontal cortex	Inferior frontal gyrus, insula	L	210	-52	20	-4	4.08	0.002
Orbitofrontal cortex	Temporal pole	L	-	-42	18	-15	2.39	0.028
Superior frontal gyrus	-	R	172	28	64	-2	3.14	0.007
Insula	Frontal operculum cortex	L	106	-40	20	4	2.67	0.015
Superior frontal gyrus	-	R	66	6	62	-22	2.49	0.028
Superior frontal gyrus	-	R	-	15	66	-18	2.28	0.038
Middle frontal gyrus	Orbitofrontal cortex	L	114	-45	50	-10	2.43	0.028
Middle frontal gyrus	-	L	-	-45	56	-4	2.41	0.022
Inferior frontal gyrus	-	R	70	36	39	-20	2.26	0.031

Note. All FTLD subtypes included. All clusters are reported at TFCE, FDR-corrected $p < .05$, 50 contiguous voxels threshold. Peak region relates to the coordinates displayed in the table; associate regions are within the cluster. Covariates included group (FTLD vs control), scanner, and TIV.

FTLD subtypes

We repeated our main analyses investigating cardiovascular risk while controlling for FTD subtypes (i.e., bvFTD, nfvPPA, svPPA, and CBS/PSP or FTD MND) to ensure that our results were not driven by the combination of FTD subtypes. Here, we replicated our main results, showing that increased cardiovascular risk was associated with AIN structures such as the bilateral insula, thalamus, amygdala, and hippocampus (Supplementary Table 17).

Supplementary Table 17. Brain regions associated with cardiovascular risk in FTLD, controlling for FTLD subtype, scanner, and TIV.

				MNI				
Peak region	**Association regions**	**Side**	**Size**	**X**	**Y**	**Z**	**t**	**FDR *p***
Insula	Heschl's gyrus, rolandic operculum	R	9075	45	-15	9	6.95	0.002
Hippocampus	Thalamus, amygdala, parahippocampal gyrus,	R	-	16	-33	-4	5.47	0.002
Hippocampus	Thalamus	R	-	36	-36	-4	5.39	0.002
Hippocampus	Parahippocampal gyrus, thalamus	L	2651	-21	-42	-8	5.93	0.002
Hippocampus	Parahippocampus	L	-	-34	-39	-4	4.78	0.002
Hippocampus	Thalamus	L	-	-15	-38	0	4.75	0.002
Mid cingulate cortex	Anterior cingulate cortex, posterior cingulate cortex	R	9433	2	-24	46	5.81	0.002
Mid cingulate cortex	Anterior cingulate cortex, posterior cingulate cortex	R	-	6	-16	48	5.49	0.002
Mid cingulate cortex	Anterior cingulate cortex, posterior cingulate cortex	R	-	2	20	38	4.93	0.002
Insula	Rolandic operculum, parietal operculum	L	277	-38	-22	14	4.49	0.002
Insula	Parietal operculum	L	-	-36	-28	20	4.01	0.003
Insula	Heschl's gyrus	L	-	-46	-10	4	3.59	0.004
Inferior frontal gyrus	Orbitofrontal cortex, frontal operculum	L	222	-52	20	-4	4.02	0.002
Orbitofrontal cortex	Insula, superior temporal gyrus	L	-	-42	18	-15	2.45	0.025
Orbitofrontal cortex	-	R	200	28	64	-2	3.21	0.006
Insula	Frontal operculum cortex, inferior frontal gyrus	L	152	-40	20	4	2.8	0.011
Orbitofrontal cortex	-	L	188	-45	56	-4	2.56	0.018
Orbitofrontal cortex	-	L	-	-46	50	-10	2.54	0.022

Orbitofrontal cortex	-	L	-	-48	48	-2	2.19	0.042
Orbitofrontal cortex	-	R	74	6	62	-22	2.54	0.028
Orbitofrontal cortex	-	R	-	15	66	-18	2.38	0.03

Note. All clusters are reported at TFCE, FDR-corrected $p < .05$, 50 contiguous voxels threshold. Regions labelled with AAL2 atlas. Covariates included group (FTD subtype vs control), scanner, and TIV.

Supplementary Table 18. Structural correlates associated with cardiovascular risk in AD.

Peak region	Association regions	Side	Size	MNI			t	FDR *p*
				X	Y	Z		
Amygdala	Parahippocampal gyrus, olfactory cortex, temporal pole, superior temporal gyrus, putamen, orbitofrontal cortex (medial and posterior), rectus, hippocampus, insula, thalamus, anterior and posterior cingulate cortex, and precuneous bilaterally	R	43986	21	4	-18	7.65	0.001
Rectus	Orbitofrontal cortex, superior frontal gyrus	L	-	-9	30	-24	7.52	0.001
Amygdala	Olfactory cortex, temporal pole, superior temporal gyrus, Insula, orbitofrontal cortex (medial and posterior), parahippocampal gyrus, putamen, rectus	L	-	-24	4	-18	7.43	0.001
Middle frontal gyrus	Superior frontal gyrus, inferior frontal gyrus, frontal pole	L	168	-44	56	-2	2.35	0.015
Middle frontal gyrus	Orbitofrontal cortex (lateral and anterior), inferior frontal gyrus, superior frontal gyrus, frontal pole	L	-	-42	50	-9	2.34	0.017

Note. All Alzheimer's presentations included (typical and atypical). All clusters are reported at TFCE, FDR-corrected $p < .05$, 50 contiguous voxels threshold. Peak region relates to the coordinates displayed in the table; associate regions are within the cluster. Covariates included group (AD vs control), scanner, and TIV.

AD subtypes

We repeated our main analyses controlling for AD subtype (typical amnestic AD, and atypical AD variants: frontal-variant AD, posterior cortical atrophy, logopenic variant primary progressive aphasia). Here, we replicated our main results, with reduced grey matter integrity in the bilateral amygdala, hippocampus, parahippocampal gyrus, superior temporal gyrus, temporal pole, insula, thalamus, anterior cingulate and paracingulate cortex were associated with higher cardiovascular risk scores in AD, controlling for AD subtypes (Supplementary Table 19).

Supplementary Table 19. Brain regions associated with cardiovascular risk in AD, controlling for AD subtype, scanner, and TIV.

Peak region	Association regions	Side	Size	MNI			t	FDR *p*
				X	Y	Z		
Amygdala	Hippocampus, thalamus, parahippocampal gyrus, insula, Heschl's gyrus, middle frontal gyrus, anterior cingulate cortex, posterior cingulate cortex	R	45381	21	4	-18	7.68	0.001
Orbitofrontal cortex (superior)	Parahippocampal gyrus, Insula, thalamus, amygdala, hippocampus	L		-9	30	-24	7.48	0.001
Amygdala	Hippocampus, parahippocampal gyrus	L		-24	4	-18	7.37	0.001
Thalamus	-	R	88	21	-15	-2	3.44	0.001
Orbitofrontal cortex (middle)	-	L	257	-42	50	-9	2.52	0.012
Middle frontal gyrus	-	L		-44	56	-2	2.5	0.010

Note. All clusters are reported at TFCE, FDR-corrected $p < .05$, 50 contiguous voxels threshold. Regions labelled with AAL2 atlas. Covariates included group (AD subtype vs control), scanner, and TIV.

Supplementary Table 20. Reduced structural integrity associated with greater cardiovascular risk in FTLD than in AD.

				MNI				
Peak region	**Associated regions**	**Side**	**Size**	**X**	**Y**	**Z**	***t***	***FDR p***
Insula	Heschl's gyrus	R	164	42	-12	6	5.15	<.001
Insula	OFC	R	-	48	15	-8	4.87	<.001
Insula	Rolandic operculum	R	-	51	9	-3	4.73	<.001
ACC	ACC	Bi	129	0	51	3	4.98	<.001
ACC	ACC	L	-	-2	48	15	4.74	<.001
ACC	ACC	R	-	2	40	24	4.16	<.001

Note. All clusters are reported at TFCE, FDR-corrected p <.05, 50 contiguous voxels threshold. Peak region relates to the coordinates displayed in the table; associate regions are within the cluster. Covariates included TIV. Abbreviations: ACC, Anterior cingulate cortex; OFC, Orbitofrontal cortex.

Functional neuroimaging results

Supplementary Table 21. Reduced functional connectivity associated with increased cardiovascular risk in FTLD.

Cluster	*F*	*p*	Connections	*t*	*p*
1	17.06	0.001	Insula R – Insula L	-4.13	<0.001
2	15.16	0.002	Thalamus R – Thalamus L	-3.89	<0.001
3	4.45	0.022	Parahippocampal L – Orbitofrontal (medial) R	-4.26	<0.001
-	-	-	Orbitofrontal (medial) R - Parahippocampal L	-4.26	<0.001
-	-	-	Orbitofrontal (medial) R - Parahippocampal R	-3.57	0.0012
-	-	-	Parahippocampal R - Orbitofrontal (medial) R	-3.57	0.0012
-	-	-	Parahippocampal L - Orbitofrontal (medial) L	-3.26	0.0060
-	-	-	Orbitofrontal (medial) R – Hippocampus R	-3.02	0.0013
-	-	-	Orbitofrontal (medial) L – Parahippocampal L	-3.26	0.0060
-	-	-	Orbitofrontal (medial) R – Hippocampus L	-2.80	0.0027
-	-	-	Hippocampus L – Orbitofrontal (medial) R	-2.80	0.0027
-	-	-	Orbitofrontal (medial) L – Hippocampus R	-2.66	0.0040
-	-	-	Hippocampus R – Orbitofrontal (medial) R	-3.02	0.0013
-	-	-	Hippocampus R – Orbitofrontal (medial) L	-2.66	0.0041
-	-	-	Parahippocampal R – Orbitofrontal (medial) L	-2.17	0.0152
4	3.96	0.038	Parahippocampal L – Orbitofrontal (superior) R	-3.75	<0.001
-	-	-	Orbitofrontal (superior) R – Parahippocampal L	-3.75	<0.001
-	-	-	Parahippocampal L – Orbitofrontal (middle) R	-2.52	0.0060
-	-	-	Parahippocampal L – Orbitofrontal (inferior) R	-2.36	0.0093
-	-	-	Parahippocampal R – Orbitofrontal (superior) R	-2.55	0.0055
5	4.45	0.038	Middle cingulate L – Posterior cingulate L	-2.83	0.0024
-	-	-	Middle cingulate R – Posterior cingulate R	-2.66	0.0040
6	7.43	0.049	Orbitofrontal (medial) R – Orbitofrontal (medial) L	-2.73	0.0030
-	-	-	Orbitofrontal (medial) L – Orbitofrontal (medial) R	-2.73	0.0030

Note. ROI-to-ROI functional connectivity results are displayed. FDR p values shown at the cluster and ROI level.

Supplementary Table 22. Reduced functional connectivity associated with increased cardiovascular risk in AD.

Cluster	*F*	*p*	Connections	*t*	*p*
1	5.09	0.021	Parahippocampal R - Orbitofrontal (medial) R	-3.94	<0.001
-	-	-	Orbitofrontal (medial) R - Parahippocampal R	-3.94	<0.001
-	-	-	Orbitofrontal (medial) R - Parahippocampal L	-3.67	<0.001
-	-	-	Parahippocampal L - Orbitofrontal (medial) R	-3.67	<0.001
-	-	-	Parahippocampal R - Orbitofrontal (medial) L	-3.39	<0.001
-	-	-	Parahippocampal L - Orbitofrontal (medial) L	-2.93	0.0017
-	-	-	Orbitofrontal (medial) L - Parahippocampal R	-3.39	<0.001
-	-	-	Orbitofrontal (medial) R - Hippocampus R	-2.89	0.0020
-	-	-	Orbitofrontal (medial) L - Parahippocampal L	-2.93	0.0017
-	-	-	Hippocampus R - Orbitofrontal (medial) R	-2.89	0.0020
2	4.30	0.043	Parahippocampal L - Orbitofrontal (middle) R	-3.65	<0.001
-	-	-	Parahippocampal R - Orbitofrontal (middle) R	-3.52	<0.001
-	-	-	Orbitofrontal (middle) R - Parahippocampal L	-3.65	<0.001
-	-	-	Orbitofrontal (middle) R - Parahippocampal R	-3.52	<0.001
-	-	-	Parahippocampal L - Orbitofrontal (superior) R	-3.09	0.0010
-	-	-	Orbitofrontal (superior) R - Parahippocampal L	-3.09	0.0010

Note. ROI-to-ROI functional connectivity results are displayed. FDR p values shown at the cluster and ROI level.

Supplementary Reference list

1. D'Agostino Sr RB, Vasan RS, Pencina MJ, Wolf PA, Cobain M, Massaro JM, et al. (2008): General cardiovascular risk profile for use in primary care: the Framingham Heart Study. *Circulation*. 117:743-753.
2. Nieto-Castanon A. Handbook of functional connectivity magnetic resonance imaging methods in CONN: Hilbert Press; 2020.
3. Friston KJ, Williams S, Howard R, Frackowiak RS, Turner R. Movement-related effects in fMRI time-series. Magnetic resonance in medicine. 1996;35(3):346-55.
4. Power JD, Mitra A, Laumann TO, Snyder AZ, Schlaggar BL, Petersen SE. Methods to detect, characterize, and remove motion artifact in resting state fMRI. Neuroimage. 2014;84:320-41.
5. Hallquist MN, Hwang K, Luna B. The nuisance of nuisance regression: spectral misspecification in a common approach to resting-state fMRI preprocessing reintroduces noise and obscures functional connectivity. Neuroimage. 2013;82:208-25.
6. Behzadi Y, Restom K, Liau J, Liu TT. A component based noise correction method (CompCor) for BOLD and perfusion based fMRI. Neuroimage. 2007;37(1):90-101.
7. Chai XJ, Castañón AN, Öngür D, Whitfield-Gabrieli S. Anticorrelations in resting state networks without global signal regression. Neuroimage. 2012;59(2):1420-8.
8. Nieto-Castanon A. Preparing fMRI data for statistical analysis. arXiv preprint arXiv:221013564. 2022.
9. Rolls ET, Joliot M, Tzourio-Mazoyer N. Implementation of a new parcellation of the orbitofrontal cortex in the automated anatomical labeling atlas. Neuroimage. 2015;122:1-5.